Geophysical Journal International

Geophys. J. Int. (2021) **225,** 354–377
Advance Access publication 2020 December 8
GJI General Geophysical Methods

doi: 10.1093/gji/ggaa584

Stability of discrete schemes of Biot's poroelastic equations

Y. Alkhimenkov [1,2,3], L. Khakimova [3,4] and Y.Y. Podladchikov [1,2,3]

[1] *Institute of Earth Sciences, University of Lausanne, Lausanne, Switzerland. E-mail: yury.alkhimenkov@unil.ch*
[2] *Swiss Geocomputing Center, University of Lausanne, Lausanne, Switzerland*
[3] *Faculty of Mechanics and Mathematics, Lomonosov Moscow State University, Moscow* 119991, *Russia*
[4] *Skoltech Center for Hydrocarbon Recovery, Skolkovo Institute of Science and Technology, Moscow, Russia*

Accepted 2020 December 4. Received 2020 October 2; in original form 2020 July 17

SUMMARY

The efficient and accurate numerical modelling of Biot's equations of poroelasticity requires the knowledge of the exact stability conditions for a given set of input parameters. Up to now, a numerical stability analysis of the discretized elastodynamic Biot's equations has been performed only for a few numerical schemes. We perform the von Neumann stability analysis of the discretized Biot's equations. We use an explicit scheme for the wave propagation and different implicit and explicit schemes for Darcy's flux. We derive the exact stability conditions for all the considered schemes. The obtained stability conditions for the discretized Biot's equations were verified numerically in one-, two- and three-dimensions. Additionally, we present von Neumann stability analysis of the discretized linear damped wave equation considering different implicit and explicit schemes. We provide both the Matlab and symbolic Maple routines for the full reproducibility of the presented results. The routines can be used to obtain exact stability conditions for any given set of input material and numerical parameters.

Key words: Numerical modelling; Seismic attenuation; Theoretical seismology; Wave propagation.

1 INTRODUCTION

Poroelasticity is a well established discipline that describes the interaction between the deformation of an elastic porous solid and the fluid flow in a porous material. Poroelastic response of an isotropic two phase medium results in two longitudinal waves (Frenkel 1944), the *P* wave of the first kind (fast) and the *P* wave of the second kind (slow), and in one shear wave. Biot (1941, 1956a,b, 1962) established poroelasticity as a discipline, which includes static and dynamic responses of a porous material, the experiments to obtain the material parameters (Biot & Willis 1957), the extensions to include viscoelasticity and non-linear behaviour of a porous material (Biot 1965). The theory of poroelasticity finds applications in many areas, including earth sciences, biology, medicine and others. In earth sciences, simplified models based on poroelasticity can be useful to induced seismicity, seismic exploration, hydrogeology, rock physics and others. Therefore, efficient and accurate numerical solutions of poroelastic equations are of great importance.

The simplest equation which describes the propagation of acoustic waves in a fluid flowing through a porous medium is called the linear damped wave equation (DWE) and is known far before the Biot's equations were introduced (Pascal 1986). The DWE describes many physical systems. This equation initially was used in the description of the telegraph, today known as the telegraph equation (Jordan & Puri 1999). The DWE also arises in the generalized (or hyperbolic) thermoelasticity (Hetnarski & Ignaczak 1999). The numerical solutions of DWE were presented in different branches of mathematics and physics. DWE (as a hyperbolic conservation law with a stiff source term) was extensively studied by many authors (Jin & Levermore 1996; Pareschi & Russo 2005; Boscarino & Russo 2013, and the references therein). Many finite difference schemes were introduced (e.g. Mickens & Jordan 2004; Mohanty 2004; Macías-Díaz & Puri 2010; Ding *et al.* 2012; Najafi & Izadi 2014). The dynamic Biot's equations of poroelasticity are far more complicated than the DWE, and researchers used different numerical methods to solve them. A finite-differences/volumes on Cartesian space-time grids were the first numerical methods used to simulate poroelastic wave propagation (Zhu & McMechan 1991; Dai *et al.* 1995; Carcione & Quiroga-Goode 1995; Özdenvar & McMechan 1997; Zeng *et al.* 2001; Masson *et al.* 2006; Wenzlau & Müller 2009; Chiavassa *et al.* 2010; Chiavassa & Lombard 2011). Other numerical solutions include pseudo-spectral methods (Özdenvar & McMechan 1997), spectral element methods (Morency & Tromp 2008), discontinuous Galerkin methods (de la Puente *et al.* 2008; Ward *et al.* 2017; Zhan *et al.* 2019; Shukla *et al.* 2020) and finite volume methods on unstructured grids (Lemoine *et al.* 2013; Lemoine 2016). Many studies have been performed for space–time finite element methods for hyperbolic (wave propagation) and parabolic problems (Schieweck 2010; Köcher & Bause 2014; Ernesti & Wieners 2019;

Bause *et al.* 2020) and the references therein. A splitting scheme has been investigated for the numerical approximation of simplified Biot's equations considering mixed hyperbolic–parabolic structure (Bause *et al.* 2019, see also Kolesov *et al.* 2014, and the references therein). Moczo *et al.* (2019) and Gregor *et al.* (2021) analyzed the accuracy of the discrete representation of material heterogeneities and subcell–resolution for the finite-difference modelling of Biot's equations.

Despite the number of numerical studies, the precise stability conditions were determined only for a few numerical schemes. The first studies profited from approximate stability conditions or investigated a stable time step numerically. Carcione & Quiroga-Goode (1995) discussed the stability issues in explicit schemes of Biot's equations. Masson *et al.* (2006) investigated the stability condition of a particular numerical scheme for Biot's equations. Chiavassa *et al.* (2010) reported the exact limits of a stable time step for the explicit schemes. O'Brien (2010) explored the stability conditions of two numerical schemes for Biot's equations and found some inconsistencies in the previous studies. Nevertheless, there are no studies which explore the stability conditions of a range of implicit and explicit schemes for the elastodynamic Biot's equations of poroelasticity and provide closed form expressions to evaluate a stable time step for any given set of material and numerical parameters. An exact stability condition for the time step is the key parameter which helps to control the accuracy and computational efficiency of numerical solutions.

In this work, we perform a rigorous von Neumann stability analysis of the discretized Biot's poroelastic equations. We use an explicit numerical scheme for the wave propagation (Virieux & Madariaga 1982; Virieux 1986) and three schemes (explicit, implicit–explicit and implicit) for Darcy's flux. Momentum conservation is exact for the applied staggered scheme for the wave propagation, momentum conservation is also satisfied after the discretization. We also perform a rigorous von Neumann stability analysis of the discretized DWE since they behave similarly to the original Biot's poroelastic equations and can help in understanding the stability of the latter. All our derivations are exact (if not mentioned otherwise) and were verified with the help of the symbolic math computing environment Maple 2019. Where it was possible, we provide the closed-form expressions for the stability conditions. Where it was not possible, we refer to the Maple script (supplementary material) where an exact stability condition can be calculated symbolically for any set of input material parameters. We also provide simple approximate expressions for the von Neumann stability of the discretized Biot's poroelastic equations for all considered schemes. Furthermore, we discuss other implicit schemes which may provide different stability conditions for the DWE and Biot's equations. We have not used any specialized terminology from the numerical analysis, thus, this article is suitable for scientists across the disciplines. For the reproducibility of the presented results, we provide both the Matlab and symbolic Maple routines. These routines are available for download from Bitbucket at https://bitbucket.org/yalkhimenkov/biotcfl/ (last access: 4 December 2020). The routines archive (v1.0) is available from a permanent DOI repository (Zenodo) (Alkhimenkov *et al.* 2020) at http://doi.org/10.5281/zenodo.4304965 (last access: 4 December 2020).

The paper is organized as follows. In Section 2, we briefly outline the theory of the von Neumann stability analysis. In Section 3, we perform the von Neumann stability analysis of the discretized DWE. In Section 4, we perform the von Neumann stability analysis of the discretized Biot's equations of poroelasticity for different discretization schemes. In Sections 5–7, we summarize the results and compare them with previous studies.

2 THEORY

The goal of a numerical solution of a partial differential equation (PDE) is to get the result, which is very close to the exact solution of the original 'continuous' PDE. In order to achieve that, a desired PDE is discretized on a certain space and time mesh and, then, the discrete version of the PDE is solved on a computer. The validity of the obtained numerical solution can be evaluated using a very well established theory of numerical methods, well explained in many text books, for example, in Hirsch (1988).

The basic idea of the numerical analysis is to evaluate several aspects of a discrete PDE (can be also called as a discretization scheme), namely, consistency, stability, convergence and accuracy. Consistency evaluates how well the discrete PDE approximates the exact (continuous) PDE. It can be done by analysing the so-called truncation error, which roughly corresponds to a Taylor expansion of the discrete PDE and evaluation of the difference between the exact solution and the discrete solution. Stability evaluates the errors of the discrete PDE as it evolves in time. It can be done by calculating the evolution of all errors (decomposed into harmonics) made at one discrete time step. Evolution of all components must be bounded otherwise the errors will be amplified at each time step. Convergence states that the numerical solution approach the exact solution of the exact (continuous) PDE as space and time discretization tend to zero. The three definitions mentioned above are related via the Lax Equivalence Theorem. This theorem states that if the discretization scheme of a well-posed linear initial value problem is consistent and stable, the scheme is convergent. The accuracy of a discretization scheme defines how fast the numerical solution tends to the exact solution as space or time discretization are reduced by an order of magnitude. The accuracy can be, for example, second order in space and second order in time, meaning that if one refines the spatial and time discretization grids by one order of magnitude, the numerical solution will become closer to the exact solution by two orders of magnitude.

2.1 Basic theory for von Neumann stability analysis

Let us consider a 1-D first order system of PDEs

$$\partial_t f(x,t) + A\,\partial_x f(x,t) = 0, \tag{1}$$

where A is a linear operator. For a numerical solution, a linear difference equation is needed. Let us use a rectangular time-space grid. The time is discretized as $t^l = l\Delta t$ and the spatial grid is discretized as $x_i = i\Delta x$. The PDE (1) can be written in a discrete form as

$$D_t f(x,t) + A\, D_x f(x,t) = 0, \tag{2}$$

where D_t and D_x are certain discrete time and space operators. The von Neumann stability method analyses a time evolution of a discrete numerical solution W_i^l of (2) in the frequency domain. This method provides the stability of linear schemes with constant coefficients. A discrete plane wave harmonic is inserted into the discrete numerical solution, which is represented as

$$W_i^l = Q_j^l e^{Ik\cdot x_i} = Q_j^l e^{Ik\cdot i\Delta x} = Q_j^l e^{Ii\phi}, \tag{3}$$

where Q_j^l is the amplitude of the j harmonic of W_i, I is the imaginary unit, $k = k_j$—is the wave number, i—is the mesh index and Δx is the mesh spacing, $\phi = i\Delta x$ is a phase angle. For a single harmonic wave $Q_j^l e^{Ii\phi}$, its time evolution is the same as for the full solution W_i^n. The stability criterion establishes a bound on the time evolution of any harmonic. The amplification factor is

$$F(\phi, \Delta t, \Delta x) = \frac{W^{l+1}}{W^l}. \tag{4}$$

For a single discrete equation, F is a scalar. For a system of discrete equations, F becomes a matrix. The von Neumann's necessary condition for stability assert that the spectral radius of the amplification matrix F must satisfy the following inequality

$$\lambda_\xi(F) \leqslant 1 + O(\Delta t), \tag{5}$$

where λ_ξ are the ξ eigenvalues of the amplification matrix F whose size is $\xi \times \xi$. Since, the stability condition depends on the spatial discretization Δx, the final analysis is performed using the inequality

$$\Delta t \leqslant \Delta x \cdot r, \tag{6}$$

where r is the parameter which controls what fraction of Δx must be used for stable Δt and corresponds to the most restrictive condition evaluated from (5). This stability condition (6) is known as the Courant–Friedrichs–Lewy (CFL) condition.

3 DISCRETE SCHEMES OF THE LINEAR DAMPED WAVE EQUATION

3.1 The damped linear wave equation

We consider the 1-D scalar damped linear wave equation (DWE) as a first order hyperbolic system,

$$\begin{cases} \dfrac{1}{K}\partial_t p = -\partial_x q \\ \partial_t q = -\dfrac{1}{\rho}\partial_x p - \dfrac{1}{\tau} q, \end{cases} \tag{7}$$

where p is the pressure, q is the velocity, K is the bulk modulus, ρ is the density and τ is the relaxation time.

The PDE (7) represents the hyperbolic system with a 'stiff' source term $1/\tau\, q$ in the right-hand side (R.H.S) of $(7)_2$. The system (7) is called 'stiff' if the two processes (advection and diffusion) have different characteristic timescales.

We introduce a dimensionless parameter ψ denoting the ratio of a characteristic time that wave travels $\tau_h = L^*/V$ (advection) over a characteristic relaxation time τ (diffusion)

$$\psi \equiv \frac{\tau}{\tau_h} = \frac{V\,\tau}{L^*}, \tag{8}$$

where L represents the characteristic length and V represents the wave velocity. If $\psi \ll 1$, the relaxation term is stiff (Jin & Levermore 1996).

Let us introduce a discrete version of (7) where we use a classical conservative staggered space-time grid discretization (Virieux 1986), which is equivalent to a finite volume approach (Dormy & Tarantola 1995). The pressure p is defined at the centre of a grid cell i and the velocity q is defined at the side of a grid cell $i \pm 1/2$ (q can be considered as a 'flux' through the grid cell). The temporal discretization of p corresponds to the half integer nodes $l + 1/2$ and the temporal discretization of q corresponds to the node integers l. The explicit discretization of the system (7) is

$$\begin{cases} \dfrac{1}{K}\dfrac{p_i^{l+1/2} - p_i^{l-1/2}}{\Delta t} = -\dfrac{q_{i+1/2}^l - q_{i-1/2}^l}{\Delta x} \\ \dfrac{q_{i+1/2}^{l+1} - q_{i+1/2}^l}{\Delta t} = -\dfrac{1}{\rho}\dfrac{p_{i+1}^{l+1/2} - p_i^{l+1/2}}{\Delta x} - \dfrac{1}{\tau} q_{i+1/2}^l. \end{cases} \tag{9}$$

3.1.1 The linear wave equation

If $1/\tau \equiv 0$, then the system (7) represents the wave equation and the von Neumann stability analysis for the discrete system (9) suggests that

$$\Delta t \leqslant \frac{\Delta x}{V}, \tag{10}$$

where $V = \sqrt{K/\rho}$ is the fast wave velocity.

3.1.2 The linear diffusion equation

The system (7) can also be treated as a diffusion equation. The discrete system for the diffusion equation can be derived from (9)

$$\begin{cases} \dfrac{1}{K}\dfrac{p_i^{l+1/2} - p_i^{l-1/2}}{\Delta t} = -\dfrac{q_{i+1/2}^{l} - q_{i-1/2}^{l}}{\Delta x} \\ q_{i+1/2}^{l+1} = -\dfrac{\tau}{\rho}\dfrac{p_{i+1}^{l+1/2} - p_i^{l+1/2}}{\Delta x}, \end{cases} \tag{11}$$

where the only difference in (11) from (9) is the replacement of $q_{i+1/2}^{l}$ in (9) to $q_{i+1/2}^{l+1}$ in (11). The von Neumann stability analysis for the discrete system (11) suggests that

$$\Delta t \leqslant \frac{(\Delta x)^2}{2\,D}, \tag{12}$$

where $D = K\tau/\rho$ is the diffusivity.

3.1.3 The dimensionless damped linear wave equation

For further stability analysis we will rely on a dimensionless formulation. The following replacements to the original DWE (7) are done

$$p \longrightarrow K\tilde{p}, \quad q \longrightarrow \frac{L^*}{t^*}\tilde{q}, \quad x \longrightarrow L^*\tilde{x}, \quad t \longrightarrow t^*\tilde{t}, \tag{13}$$

where L^* [m] is the characteristic length, t^* [s] is the characteristic time and the variables with the symbol $\tilde{}$ on top correspond to the dimensionless quantities. We also set $L^* = V\,t^*$ and $t^* = \tau$. The dimensionless system (7) reads

$$\begin{cases} \partial_{\tilde{t}}\,\tilde{p} = -\partial_{\tilde{x}}\,\tilde{q} \\ \partial_{\tilde{t}}\,\tilde{q} = -\partial_{\tilde{x}}\,\tilde{p} - \tilde{q}. \end{cases} \tag{14}$$

Below, we will deal only with the dimensionless equations, and, for simplicity, we will omit the over-score tilde symbol $\tilde{}$ in the rest of the paper (excluding appendices).

3.2 The discrete system of equations

Let us consider a more general discrete system than (9) where we will use the fact that there are no spatial derivatives of the field $q_{i+1/2}^{l}$ in R.H.S of $(14)_2$. Thus, $q_{i+1/2}^{l}$ can be replaced as a weighted average between the future $q_{i+1/2}^{l+1}$ and the past $q_{i+1/2}^{l}$ values,

$$\begin{cases} \dfrac{p_i^{l+1/2} - p_i^{l-1/2}}{\Delta t} = -\dfrac{q_{i+1/2}^{l} - q_{i-1/2}^{l}}{\Delta x} \\ \dfrac{q_{i+1/2}^{l+1} - q_{i+1/2}^{l}}{\Delta t} = -\dfrac{p_{i+1}^{l+1/2} - p_i^{l+1/2}}{\Delta x} - \left(\chi\, q_{i+1/2}^{l+1} + (1-\chi)\, q_{i+1/2}^{l}\right). \end{cases} \tag{15}$$

If $\chi = 1/2$, the scheme (15) corresponds to an implicit–explicit scheme. If $\chi = 1$, the scheme (15) corresponds to an implicit scheme for q. The schemes with $\chi = 1/2$ ans with $\chi = 1$, even though are implicit for q, can be executed fully explicitly. The consistency is shown in many studies, for example, in Najafi & Izadi (2014) and references therein. Our numerical tests show that all three schemes described above (explicit, implicit–explicit, implicit) under a sufficient resolution converge to the same numerical solution using homogeneous and heterogeneous material properties.

A typical behaviour of the system (14) is shown in Fig. 1. The wave propagation regime of DWE corresponds to a propagating wave (left and right going wavelets with the same velocities), which is equivalent to a standard wave equation (Fig. 1a). The diffusion regime of DWE corresponds to a diffusion event, which is equivalent to the standard diffusion equation (Fig. 1b).

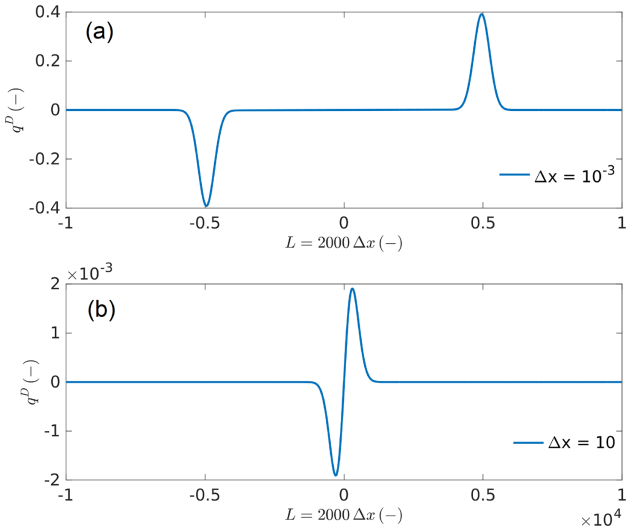

Figure 1. Snapshots of the velocity wave fields of DWE (14). Panel (a) shows one propagating wave, which corresponds to the wave propagation regime of DWE. Panel (b) shows a diffusive mode, which corresponds to the diffusive regime of DWE. We apply a Gaussian distribution to the pressure p at the centre of the model as an initial condition.

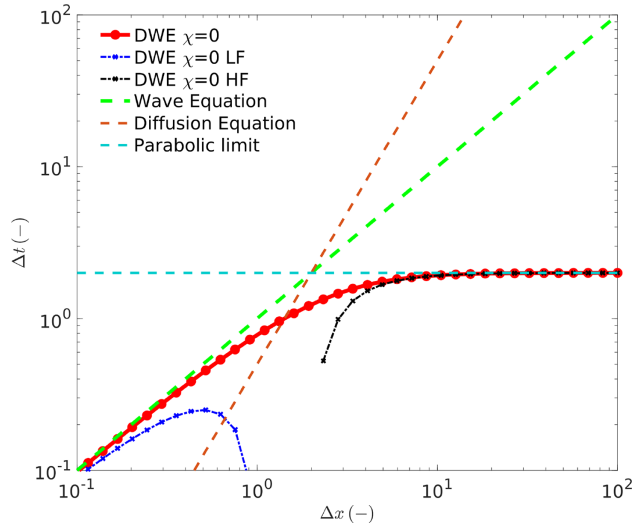

Figure 2. The CFL condition Δt as a function of Δx for the explicit scheme ($\chi = 0$) (red curve), its wave equation limit ($\Delta x \ll 1$) (blue curve), its parabolic limit (black curve), the standard wave equation (dashed green curve), the diffusive equation (dashed brown curve) and the parabolic limit (dashed light blue curve).

3.3 The explicit scheme

Here, we explore the discrete system (15) with $\chi = 0$, which corresponds to the explicit scheme. The von Neumann stability analysis for this scheme suggests that

$$\Delta t \leqslant \Delta x \frac{-\Delta x + \sqrt{(\Delta x)^2 + 16}}{4}, \tag{16}$$

The behaviour of this stability condition as a function of Δx is shown in Fig. 2 (solid red curve). Let us analyse the result (16) in more detail.

3.3.1 Wave propagation regime of the damped linear wave equation

Lets us write a series expansion of the R.H.S. of (16) of Δx, assuming $\Delta x \ll 1$,

$$\Delta x \frac{-\Delta x + \sqrt{(\Delta x)^2 + 16}}{4} = \Delta x - \frac{1}{4}(\Delta x)^2 + \frac{1}{32}(\Delta x)^3 + O((\Delta x)^5). \tag{17}$$

It can be seen form (17) that the limit of (17) as $\Delta x \to 0$ is

$$\lim_{\Delta x \to 0} \left(\Delta x \frac{-\Delta x + \sqrt{(\Delta x)^2 + 16}}{4} \right) = 0, \tag{18}$$

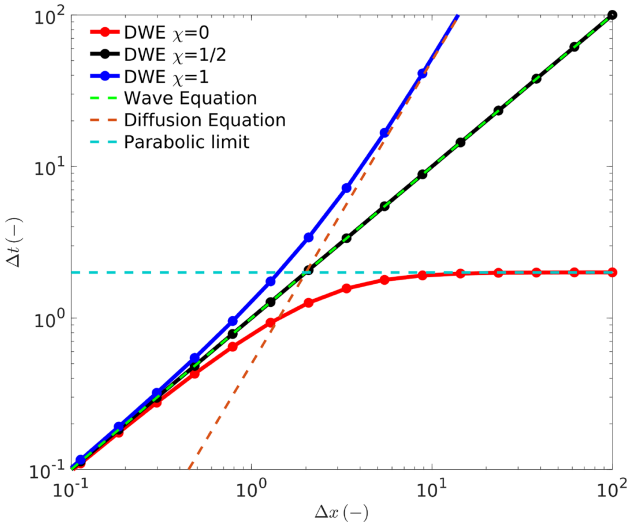

Figure 3. The CFL condition Δt as a function of Δx for the explicit scheme ($\chi = 0$) (red curve), the implicit–explicit scheme ($\chi = 0.5$) (black curve), the implicit scheme ($\chi = 1$) (blue curve), the standard wave equation (dashed green curve), the diffusive equation (dashed brown curve) and the parabolic limit (dashed light blue curve).

which corresponds to the hyperbolic limit. Indeed, taking into account (17), the inequality (16) can be written as

$$\Delta t \leqslant \Delta x, \tag{19}$$

which is valid when $\Delta x \ll 1$ (Fig. 2, dashed green curve). This CFL condition is indeed corresponds to the CFL of the wave eq. (10), because the velocity equals to 1. One can also take into account one more term in the series expansion (17) and the inequality (19) becomes

$$\Delta t \leqslant \Delta x - \frac{1}{4}(\Delta x)^2, \tag{20}$$

which is shown in Fig. 2 (dotted blue curve).

3.3.2 Diffusive regime of the damped linear wave equation

Now we consider an opposite scenario. We write a series expansion of the R.H.S of (16) of $1/\Delta x$, assuming $1/\Delta x \ll 1$,

$$\Delta x \frac{-\Delta x + \sqrt{(\Delta x)^2 + 16}}{4} = 2 - \frac{8}{(\Delta x)^2} + \frac{64}{(\Delta x)^4} + O(\frac{1}{(\Delta x)^6}). \tag{21}$$

The limit of the R.H.S. of (21) as $\Delta x \to +\infty$ is

$$\lim_{\Delta x \to +\infty} \left(\Delta x \frac{-\Delta x + \sqrt{(\Delta x)^2 + 16}}{4} \right) = 2 \tag{22}$$

It is interesting that the R.H.S of (22) is finite. Thus, when $\Delta x \gg 1$, the stability conditions reads

$$\Delta t \leqslant 2, \tag{23}$$

which is a parabolic limit and is shown in Fig. 2 (dashed light blue curve). One can also take into account one more term in the series expansion (21) and the inequality (23) becomes

$$\Delta t \leqslant 2 - \frac{8}{(\Delta x)^2}, \tag{24}$$

which is shown in Fig. 2 (dotted black curve).

3.4 The implicit and implicit–explicit schemes

Let us now explore the implicit–explicit scheme ($\chi = 1/2$ in (15)). The von Neumann stability analysis for this scheme suggests that

$$\Delta t \leqslant \Delta x, \tag{25}$$

which is valid for any Δx (Fig. 3, solid black curve). It means that the standard CFL for the wave eq. (7) is valid in all regimes of the system (15).

Now, we analyse the implicit scheme ($\chi = 1$ in (15)). The von Neumann stability analysis for this scheme suggests that

$$\Delta t \leqslant \Delta x \left(\frac{\Delta x}{4} + \frac{\sqrt{(\Delta x)^2 + 16}}{4} \right), \tag{26}$$

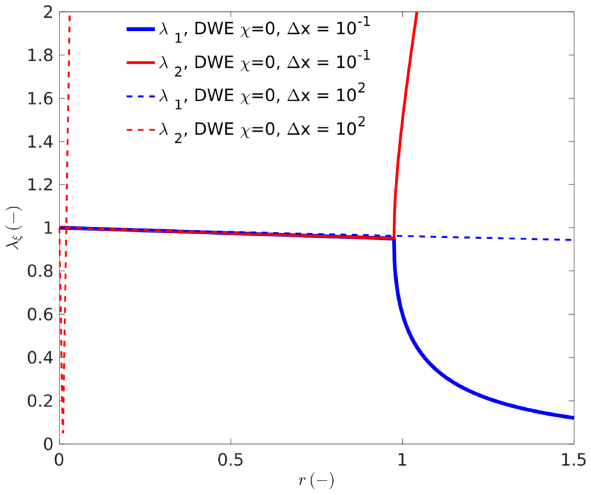

(a)

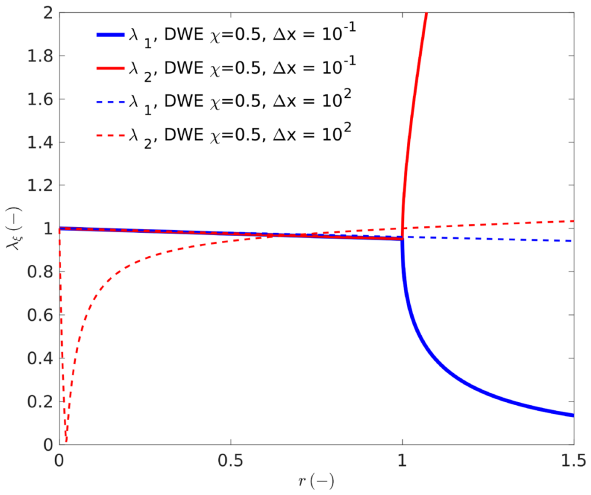

(b)

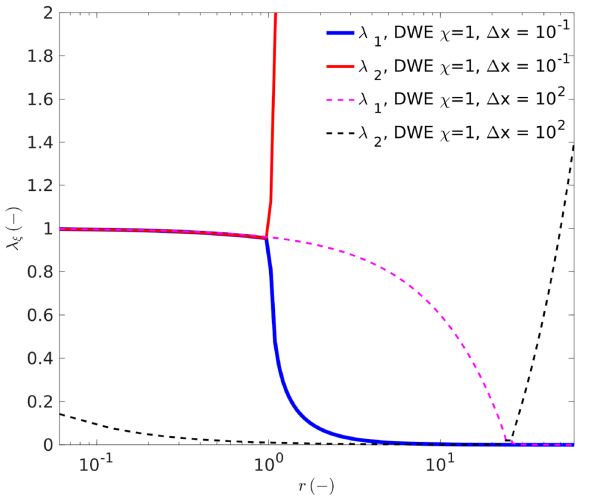

(c)

Figure 4. The eigenvalues $\lambda_{1,2}$ of the amplification matrix F for the three discrete schemes as a function of r (6). (a) explicit scheme ($\chi = 0$), (b) implicit–explicit scheme ($\chi = 0.5$) and (c) implicit scheme ($\chi = 1$). The x-axis in panels (a) and (b) is linear while the x-axis in panel (c) is logarithmic.

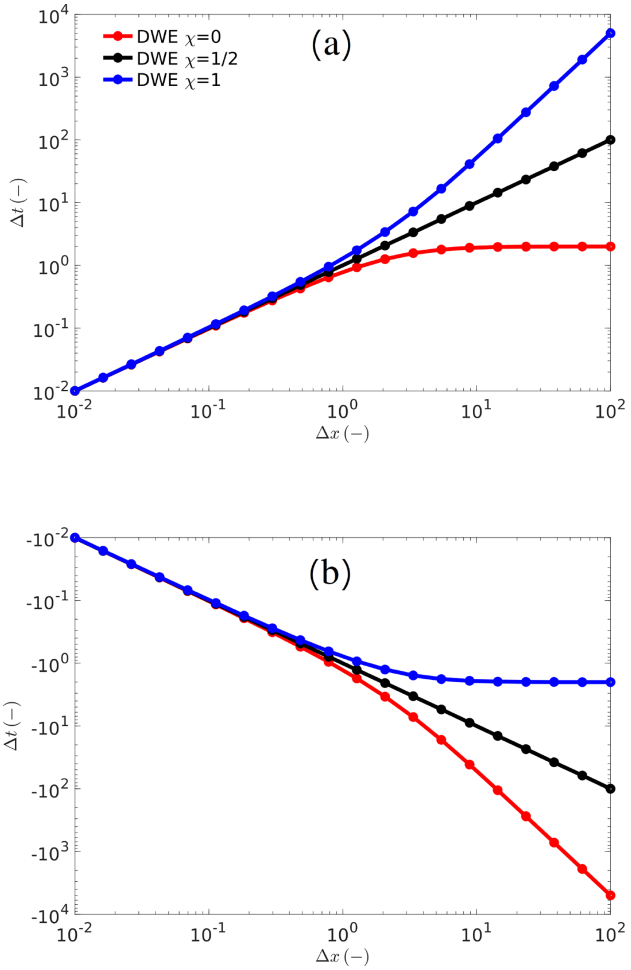

Figure 5. The CFL conditions of DWE for positive (a) and negative (b) Δt as a function of Δx for the three schemes—the explicit scheme ($\chi = 0$) (red curve), the implicit–explicit scheme ($\chi = 0.5$) (black curve), the implicit scheme ($\chi = 1$) (blue curve).

which is shown in Fig. 3 (solid blue curve). This CFL condition is equivalent to the CFL of the wave eq. (7) for $\Delta x \ll 1$ (Fig. 3, dashed green curve) and to the CFL of the diffusion eq. (12) if $\Delta x \gg 1$ (Fig. 3, dashed brown curve). For comparison, the CFL condition of the explicit scheme is also shown in Fig. 3 (solid red curve), as well as, the parabolic limit (Fig. 3, dashed light blue curve).

3.5 Summary to the CFL conditions of the linear damped wave equation

The general CFL condition of the linear damped wave equation can be written as a function of parameter χ, which defines the ratio between explicit and implicit schemes,

$$\Delta t \leqslant \Delta x \left(\frac{(2\,\chi - 1)}{4} \Delta x + \frac{\sqrt{16 + 4(\chi - \frac{1}{2})^2 (\Delta x)^2}}{4} \right). \tag{27}$$

The CFL condition (27) captures the CFL conditions for the three considered above schemes—explicit, implicit–explicit and implicit. To support the results presented above, we show the absolute values of the eigenvalues $\lambda_{1,2}$ of the amplification matrix F (4) for the three described above numerical schemes (Fig. 4). We plot the eigenvalues $\lambda_{1,2}$ for two different values of Δx. $\Delta x = 10^2$ corresponds to the diffusive regime of DWE while $\Delta x = 10^{-1}$ corresponds to the wave propagation regime of DWE. In the explicit scheme, the eigenvalue λ_2 significantly reduces the stable Δt in the diffusive regime (Fig. 4a, dashed red curve). In the implicit–explicit scheme, the eigenvalues $\lambda_{1,2}$ provide the same stability condition in the wave propagation and diffusive regimes (Fig. 4b). In the implicit scheme, the eigenvalues $\lambda_{1,2}$ provide the CFL condition (25) in the wave propagation regime and the CFL condition (12) in the diffusive regime (Fig. 4c, note a logarithmic scale of the x-axis). We also provide the von Neumann stability analysis of the dimensional linear damped wave equation which can be found in Appendix A. The corresponding Maple script for the derivation of the CFL conditions of DWE is provided as a supplementary material.

Table 1. List of principal notation.

Symbol	Meaning	Unit
σ^s, σ^f	solid and fluid stresses	–
$\bar{\sigma}$	$=(1-\phi)\sigma^s + \phi\sigma^f$, total stress	–
p_f	fluid pressure	–
v^s, v^f	solid and fluid velocities	–
q^D	$=\phi(v^f - v^s)$, Darcy's flux	–
$\tilde{\alpha}$, $\tilde{M}$, $\tilde{\varrho}_f$, $\tilde{\varrho}_t$	dimensionless material parameters specified in Appendix B	–

3.6 Back propagation of the damped linear wave equation

It is notable that the derived CFL conditions for the three schemes exhibit mirror symmetry along $\Delta t = 0$ (Fig. 5). The CFL condition of the implicit–explicit scheme is exactly the same for positive and negative Δt (Fig. 5, black curve). The CFL conditions of the explicit and implicit schemes are reciprocal (Fig. 5, red and blue curves). One of the main properties of the wave equation is the ability to propagate forward and backward in time, which is due the the hyperbolicity of the system. DWE exhibits this property as long as the propagation regime dominates. If the diffusion regime dominates, the back propagation results in growing amplitudes at each time step, thus, the back propagation solution will never converge to the initial state. Remarkably, during the back propagation the numerical schemes remain stable under the negative CFL conditions in both wave propagation and diffusion regimes.

4 DISCRETE SCHEMES OF DIMENSIONLESS BIOT'S POROELASTIC EQUATIONS

The dimensionless Biot's poroelastic equations in 1-D can be written as

$$\begin{pmatrix} \frac{\partial \bar{\sigma}}{\partial t} \\ -\frac{\partial p_f}{\partial t} \end{pmatrix} = \zeta_{ij} \begin{pmatrix} \frac{\partial v^s}{\partial x} \\ \frac{\partial q^D}{\partial x} \end{pmatrix}, \tag{28}$$

$$\begin{pmatrix} \frac{\partial v^s}{\partial t} \\ -\frac{\partial q^D}{\partial t} \end{pmatrix} = \varrho_{ij} \begin{pmatrix} \frac{\partial \bar{\sigma}}{\partial x} \\ q^D + \frac{\partial p_f}{\partial x} \end{pmatrix}, \tag{29}$$

where

$$\zeta_{ij} = \begin{pmatrix} 1 & \tilde{\alpha} \\ \tilde{\alpha} & \tilde{M} \end{pmatrix}, \quad \varrho_{ij} = \begin{pmatrix} 1 & \tilde{\varrho}_f \\ \tilde{\varrho}_f & \tilde{\varrho}_t \end{pmatrix}. \tag{30}$$

A detailed derivation of the dimensionless Biot's poroelastic eqs (28)–(29) is given in Appendix B. The list of notations is given in Table 1. The matrices of coefficients (30) define the material parameters and are positive definite and symmetric. The system (28)–(29) is called inviscid if q^D is not present in the R.H.S of (29). The inviscid system is hyperbolic and its solution results in propagating waves. If $\zeta_{ij} = a \cdot \varrho_{ij}$, where a is an arbitrary non-zero positive number, the solution of the inviscid system (28)–(29) results in one propagating wave (i.e. left and right going wavelets with the same velocities). If $\zeta_{ij} \neq a \cdot \varrho_{ij}$, then the solution of the inviscid system (28)–(29) results in two propagating waves with the two different velocities (i.e. two left and two right going wavelets).

If q^D is present in the R.H.S of (29), Biot's poroelastic eqs (28)–(29) define the hyperbolic system with a stiff source term, represented by a parabolic operator. The behaviour of such a dimensionless system of equations depends on Δx (i.e. depends on the spatial scale). If $\Delta x \ll 1$, the solution of the system (28)-(29) results in two propagating waves with the two different velocities (V_1^{HF} and V_2^{HF}) like in the case of an inviscid system (Fig. 6a). The fastest P wave is called the wave of the first kind (or fast P wave, Biot 1956a) and the second wave is called the P wave of the second kind (so-called slow P wave). The superscript 'HF' refers to the high frequency limit, since the velocities V_1^{HF} and V_2^{HF} correspond to the high frequency limit of the dimensional Biot's equations. The velocities V_1^{HF} and V_2^{HF} can be calculated as

$$V_1^{HF} = \left(\frac{A - \sqrt{A^2 - 4\det(\zeta_{ij})\det(\varrho_{ij})}}{2\det(\zeta_{ij})\det(\varrho_{ij})} \right)^{-1/2} \tag{31}$$

and

$$V_2^{HF} = \left(\frac{A + \sqrt{A^2 - 4\det(\zeta_{ij})\det(\varrho_{ij})}}{2\det(\zeta_{ij})\det(\varrho_{ij})} \right)^{-1/2}, \tag{32}$$

where the determinants are

$$\det(\zeta_{ij}) = \zeta_{11}\zeta_{22} - \zeta_{12}^2 \tag{33}$$

and

$$\det(\varrho_{ij}) = \varrho_{11}\varrho_{22} - \varrho_{12}^2. \tag{34}$$

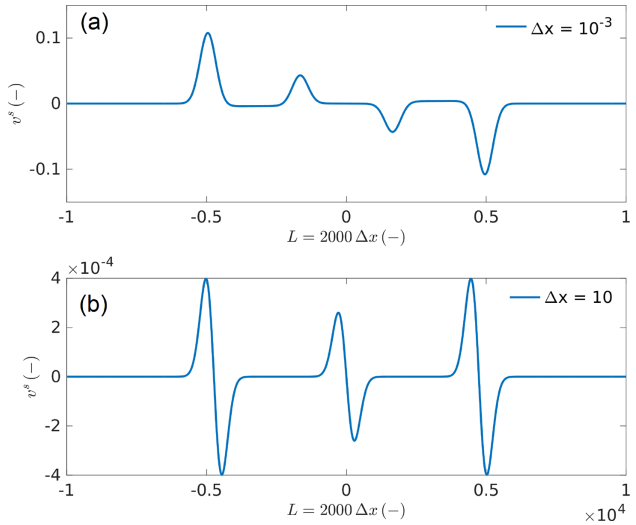

Figure 6. Snapshots of the solid velocity wavefields of the dimensionless Biot's poroelastic eqs (28)–(29). Panel (a) shows two propagating waves V_1 and V_2, which corresponds to the wave propagation regime for V_2. Panel (b) shows one propagating wave V_1 and a diffusive mode, which corresponds to V_2. The initial condition is given to the fluid pressure p_f of a Gaussian shape. The material parameters are $\zeta_{12} = 1/8$, $\zeta_{22} = 1/4$, $\varrho_{12} = 1/4$, $\varrho_{22} = 1/2$.

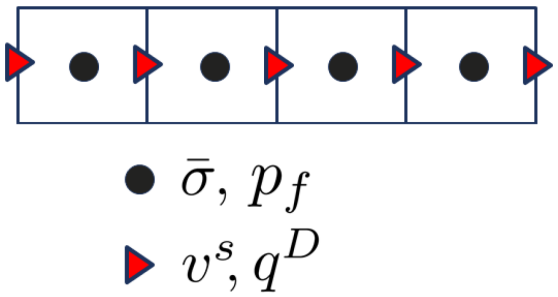

Figure 7. A sketch representing the spatial locations of the field variables of Biot's equations in a staggered mesh.

The parameter A is defined as

$$A = \zeta_{11}\varrho_{11} + \zeta_{22}\varrho_{22} - 2\zeta_{12}\varrho_{12}. \tag{35}$$

If $\Delta x \gg 1$, the solution of the system (28)–(29) results in one propagating P wave with velocity V_1^{LF} (i.e. left and right going wavelets with the same velocities) and in a slow P wave, which is degenerated into a diffusion mode (Fig. 6b). The superscript "LF" refers to the low frequency limit, since the velocities V_1^{LF} and V_2^{LF} correspond to the low frequency limit of the dimensional Biot's equations. The velocity V_1^{LF} is lower than the velocity V_1^{HF} and can be calculated as

$$V_1^{LF} = \sqrt{\frac{\zeta_{11}}{\varrho_{22}/(\varrho_{11}\varrho_{22} - \varrho_{12}^2)}}. \tag{36}$$

The discrete system of eqs (28)–(29) can be written as

$$\begin{cases} \dfrac{(\bar{\sigma})_i^{l+1/2} - (\bar{\sigma})_i^{l-1/2}}{\Delta t} = \zeta_{11}\dfrac{(v^s)_{i+1/2}^l - (v^s)_{i-1/2}^l}{\Delta x} + \zeta_{12}\dfrac{(q^D)_{i+1/2}^l - (q^D)_{i-1/2}^l}{\Delta x} \\ -\dfrac{(p_f)_i^{l+1/2} - (p_f)_i^{l-1/2}}{\Delta t} = \zeta_{21}\dfrac{(v^s)_{i+1/2}^l - (v^s)_{i-1/2}^l}{\Delta x} + \zeta_{22}\dfrac{(q^D)_{i+1/2}^l - (q^D)_{i-1/2}^l}{\Delta x} \end{cases}, \tag{37}$$

$$\begin{cases} -\dfrac{(q^D)_{i+1/2}^{l+1} - (q^D)_{i+1/2}^l}{\Delta t} = \varrho_{21}\dfrac{(\bar{\sigma})_{i+1}^{l+1/2} - (\bar{\sigma})_i^{l+1/2}}{\Delta x} + \varrho_{22}\left(\dfrac{(p_f)_{i+1}^{l+1/2} - (p_f)_i^{l+1/2}}{\Delta x} + \left(\chi\,(q^D)_{i+1/2}^{l+1} + (1-\chi)\,(q^D)_{i+1/2}^l\right)\right) \\ \dfrac{(v^s)_{i+1/2}^{l+1} - (v^s)_{i+1/2}^l}{\Delta t} = \varrho_{11}\dfrac{(\bar{\sigma})_{i+1}^{l+1/2} - (\bar{\sigma})_i^{l+1/2}}{\Delta x} + \varrho_{12}\left(\dfrac{(p_f)_{i+1}^{l+1/2} - (p_f)_i^{l+1/2}}{\Delta x} + \left(\chi\,(q^D)_{i+1/2}^{l+1} + (1-\chi)\,(q^D)_{i+1/2}^l\right)\right) \end{cases}. \tag{38}$$

The discrete system (37)–(38) corresponds to the fully explicit scheme for the wave equations, but the scheme for Darcy's flux can be different. If $\chi = 0$, the scheme for Darcy's flux is explicit. If $\chi = 1/2$, the scheme for Darcy's flux is implicit–explicit. If $\chi = 1$, the scheme for Darcy's flux is implicit. In fact, the scheme (37)–(38) can be executed always explicitly for any scheme for Darcy's flux (explicit or implicit–explicit or implicit), since Darcy's flux q^D in the R.H.S of (29) does not have any spatial derivatives. Spatial locations of different fields in the mesh are shown in Fig. 7.

We performed the stability analysis outlined in Section 2 for the system (28)–(29). For the inviscid system (28)–(29), the CFL condition is

$$\Delta t \leqslant \frac{\Delta x}{V_1}, \tag{39}$$

where V_1 is the velocity of the fastest wave. This velocity V_1 is equivalent to the velocity of the system (28)–(29) (with Darcy's flux in the R.H.S) V_1^{HF} ($\Delta x \ll 1$). In addition to the CFL condition (39), the matrices ζ_{ij} and ϱ_{ij} must be positive definite, which follows from the energy laws and, independently, from the performed stability analysis. For the stability analysis of the original viscid Biot's poroelastic eqs (28)–(29), let us consider the two examples.

4.1 Example 1

Let us set the dimensionless material parameters ζ_{ij} and ϱ_{ij} as

$$\zeta_{ij} = \begin{pmatrix} 1 & 1/2 \\ 1/2 & 1 \end{pmatrix}, \quad \varrho_{ij} = \begin{pmatrix} 1 & 1/2 \\ 1/2 & 1 \end{pmatrix}. \tag{40}$$

This set of parameters corresponds to a special condition when the velocities V_1 and V_2 are the same. The wave mode V_2 behaves as a propagating wave if $\Delta x \ll 1$ and as a diffusion mode if $\Delta x \gg 1$. The beauty of this example is that the CFL conditions for the considered above schemes can be derived fully analytically.

4.1.1 Explicit scheme for Darcy's flux

We fist consider the explicit scheme for Darcy's flux ($\chi = 0$) for the system (37)–(38). The CFL condition can be derived by reproducing the workflow presented in Section 2. The amplification matrix for this scheme is shown in Appendix C. The CFL condition states that the eigenvalues of the amplification matrix F must satisfy the inequality (5), which can be represented as a solution of

$$\gamma = |\lambda_\xi(F)| - 1, \tag{41}$$

where λ_ξ are the ξ eigenvalues of the amplification matrix F and $\xi = \overline{1..4}$. The polynomial γ is of degree four and has four roots, $\gamma_{\overline{1..4}}$. The roots are

$$\gamma_{1,2} = \pm 1/V_1^{HF}, \quad \gamma_{3,4} = -\frac{\Delta x}{3} \pm \frac{\sqrt{(\Delta x)^2 + 12}}{3}, \tag{42}$$

where $V_1^{HF} = \sqrt{3}/2 \approx 0.866$. According to (6), the resulting CFL condition can be written as

$$\Delta t \leqslant \Delta x \ \min(\gamma_{\overline{1..4}}), \tag{43}$$

where the most restrictive condition $\gamma_{\overline{1..4}}$ must be chosen. The resulting constrains on Δt are

$$\Delta t \leqslant \left|\pm \Delta x / V_1^{HF}\right|, \tag{44}$$

$$\Delta t \leqslant \left|\Delta x \left(-\frac{\Delta x}{3} \pm \frac{\sqrt{(\Delta x)^2 + 12}}{3}\right)\right|, \tag{45}$$

It can be seen from $(42)_1$ and (44) that roots $\gamma_1 = -\gamma_2$ and $\gamma_{\overline{1,2}}$ represent the stability of the inviscid set of eqs (39) (Fig. 8, solid black curve). The most restrictive condition is represented by (45) with a plus sign, thus the CFL condition of the explicit scheme ($\chi = 0$) for Biot's eqs (28)–(29) is represented by

$$\Delta t \leqslant \Delta x \left(-\frac{\Delta x}{3} + \frac{\sqrt{(\Delta x)^2 + 12}}{3}\right). \tag{46}$$

The CFL condition (46) is shown in Fig. 8 (solid red curve). The hyperbolic limit ($\Delta x \ll 1$) of the CFL condition (46) is

$$\Delta t \leqslant \Delta x \frac{2}{\sqrt{3}} \approx \Delta x / 0.866. \tag{47}$$

The parabolic limit ($\Delta x \gg 1$) of (46) is

$$\Delta t \leqslant 2, \tag{48}$$

which is shown in Fig. 8 (dashed light blue curve).

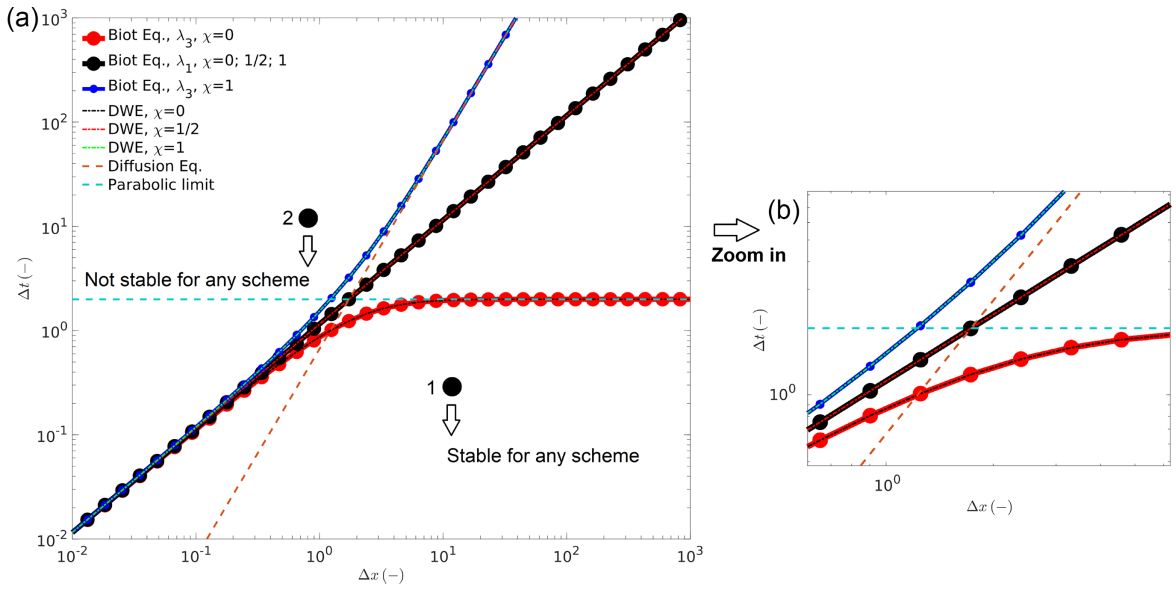

Figure 8. The restrictions on Δt arising from the roots $\gamma_{\overline{1..4}}$ as a function of Δx for Biot's and modified DWE equations considering explicit, implicit–explicit and implicit schemes for Darcy's flux. $\lambda_1 = 1$ and $\lambda_3 = 1$ correspond to the positive roots (a and b). Point 1 is stable for any scheme, point 2 is not stable for any scheme.

4.1.2 Implicit–explicit scheme for Darcy's flux

We repeat the workflow presented in Section 2 for the scheme (37)–(38) with $\chi = 1/2$ (implicit–explicit scheme for Darcy's flux). The amplification matrix for this scheme is shown in Appendix C. Again, the polynomial γ is of degree four and has four roots, $\gamma_{\overline{1..4}}$ (see 41). The resulting CFL condition of the scheme with $\chi = 1/2$ for Biot's eqs (28)–(29) can be written as

$$\Delta t \leqslant \Delta x / V_1^{HF}, \tag{49}$$

which is the most restrictive condition (Fig. 8, solid black curve) and is the same as the CFL condition of the wave eq. (10) (taking $V = V_1^{HF}$). In fact, the absolute values of all roots $\gamma_{\overline{1..4}}$ provide this stability condition.

4.1.3 Implicit scheme for Darcy's flux

We repeat the workflow presented in Section 2 for the scheme (37)-(38) with $\chi = 1$ (implicit scheme for Darcy's flux). The amplification matrix for this scheme is shown in Appendix C. The polynomial γ is of degree four and has four roots, $\gamma_{\overline{1..4}}$ (see 41). The roots are

$$\gamma_{1,2} = \pm 1/V_1^{HF}, \quad \gamma_{3,4} = \frac{\Delta x}{3} \pm \frac{\sqrt{(\Delta x)^2 + 12}}{3}, \tag{50}$$

where $V_1^{HF} = \sqrt{3}/2 \approx 0.866$. Note, that the only difference between (42) and (50) is the plus sign in (50) in front of $\Delta x/3$. The stability conditions arising from (50) with the help of (6) are

$$\Delta t \leqslant \left| \pm \Delta x / V_1^{HF} \right|, \tag{51}$$

$$\Delta t \leqslant \left| \Delta x \left(\frac{\Delta x}{3} \pm \frac{\sqrt{(\Delta x)^2 + 12}}{3} \right) \right|, \tag{52}$$

where $V_1^{HF} = \sqrt{3}/2 \approx 0.866$. The stability condition (51) (arising from $\gamma_{\overline{1,2}}$) is exactly the same as for the explicit and implicit–explicit schemes for Darcy's flux. The stability condition (52) with a plus sign is shown in Fig. 8 (solid dark blue curve). The most restrictive condition arising from (51) to (52) is

$$\Delta t \leqslant \Delta x / V_1^{HF}, \tag{53}$$

which is the same as the CFL condition of the wave eq. (10) (taking $V = V_1^{HF}$).

Table 2. Summary of CFL conditions for different schemes in Example 1.

Scheme for Darcy's flux	Explicit	Explicit–implicit	Implicit
Scheme for the wave propagation part	Explicit	Explicit	Explicit
CFL condition	$\Delta t \leqslant \Delta x \left(-\frac{\Delta x}{3} + \frac{\sqrt{(\Delta x)^2 + 12}}{3} \right)$	$\Delta t \leqslant \frac{\Delta x}{V_1^{HF}}$	$\Delta t \leqslant \frac{\Delta x}{V_1^{HF}}$

4.1.4 The modified CFL condition of the DWE

Let us sightly modify the CFL condition of the linear damped wave eq. (A11) considering the explicit scheme ($\chi = 0$),

$$\Delta t \leqslant \Delta x \frac{\frac{1}{V_1^{HF}} \sqrt{(\Delta x)^2 \frac{1}{(V_1^{HF})^2} + 16 \frac{1}{\varrho_{22}}} + \frac{1}{(V_1^{HF})^2} \Delta x}{4 \frac{1}{\varrho_{22}}}, \tag{54}$$

where for the wave velocity V in (A11), the velocity of the fist kind V_1^{HF} of Biot's eqs (28)–(29) is used. In addition, the parabolic limit is modified by a factor $1/\varrho_{22}$. The modified CFL condition of DWE with $\chi = 0$ (54) is shown in Fig. 8 (dotted black curve), which is exactly equivalent to the CFL condition of Biot's equations for the explicit scheme for Darcy's flux (46) (solid red curve in Fig. 8).

The modified CFL condition of DWE with $\chi = 1/2$ (Fig. 8, dotted red curve) is equivalent to the CFL of the wave eq. (10) (taking $V = V_1^{HF}$), Thus, it is also equivalent to the CFL condition of Biot's equations for the implicit–explicit scheme for Darcy's flux (53).

The modified CFL condition of DWE with $\chi = 1$ can be derived from (A11) applying the the same changes as above (Fig. 8, dotted green curve). This CFL condition is equivalent the CFL condition of Biot's equations arriving from the root γ_3. Note, that the modified CFL condition of the DWE with $\chi = 1$ is always less restrictive than the stability condition of the wave eq. (10) (using $V = V_1^{HF}$); thus, it does not have an effect in Biot's equations if the scheme for the hyperbolic part of Biot's equations is explicit.

The CFL condition of the diffusion eq. (12) is shown in Fig. 8 (dashed brown curve), where the diffusivity D is calculated according to

$$D = \zeta_{22} \left(1 - \frac{\zeta_{12}^2}{\zeta_{22} \zeta_{11}} \right). \tag{55}$$

This diffusivity coefficient defines the diffusion equation for the fluid pressure, which behaves exactly the same as the diffusive mode V_2 of Biot's eqs (28)–(29) for $\Delta x \gg 1$. Note, the similarities between Figs 2 and 8. The summary of CFL conditions for different schemes in Example 1 is shown in Table 2.

4.2 Example 2

Let us set the dimensionless material parameters ζ_{ij} and ϱ_{ij} as

$$\zeta_{ij} = \begin{pmatrix} 1 & 1/8 \\ 1/8 & 1/4 \end{pmatrix}, \quad \varrho_{ij} = \begin{pmatrix} 1 & 1/4 \\ 1/4 & 1/2 \end{pmatrix} \tag{56}$$

This set of parameters corresponds to the different velocities V_1 and V_2. In this example, the wave mode V_2 behaves as a propagating wave if $\Delta x \ll 1$ and as a diffusion mode if $\Delta x \gg 1$. The CFL condition can be written analytically as a root of a polynomial of degree four. The roots can be easily found numerically. We briefly repeat a similar workflow for this set of parameters as we performed in Example 1.

4.2.1 Explicit scheme for Darcy's flux

We again fist consider the explicit scheme ($\chi = 0$) for Darcy's flux (28)-(29). For this scheme, the CFL condition can be written as

$$\Delta t \leqslant \Delta x \ \min|\gamma_\xi(z)|, \tag{57}$$

where γ_ξ are the four roots ($\xi = \overline{1..4}$) of the polynomial γ

$$\gamma(z) = 4(105z^4 + 56\Delta x\, z^3 - 68z^2 - 4\Delta x\, z + 4). \tag{58}$$

The roots of (58) obey a similar behaviour as in Example 1. The most restrictive condition is arriving from $\gamma_{3,4}$ (Fig. 9, solid red curve). The hyperbolic limit ($\Delta x \ll 1$) of the CFL condition arriving from $\gamma_{1,2}$ is (here, we consider γ_1, since it corresponds to the positive Δt)

$$\Delta t \leqslant \Delta x / V_1^{HF}, \tag{59}$$

where $V_1^{HF} \approx 0.977$ (Fig. 9, solid black curve). The parabolic limit ($\Delta x \gg 1$) of the CFL condition arriving from $\gamma_{3,4}$ is (here, we consider γ_3, since it corresponds to the positive Δt)

$$\Delta t \leqslant \frac{2}{\varrho_{22}}. \tag{60}$$

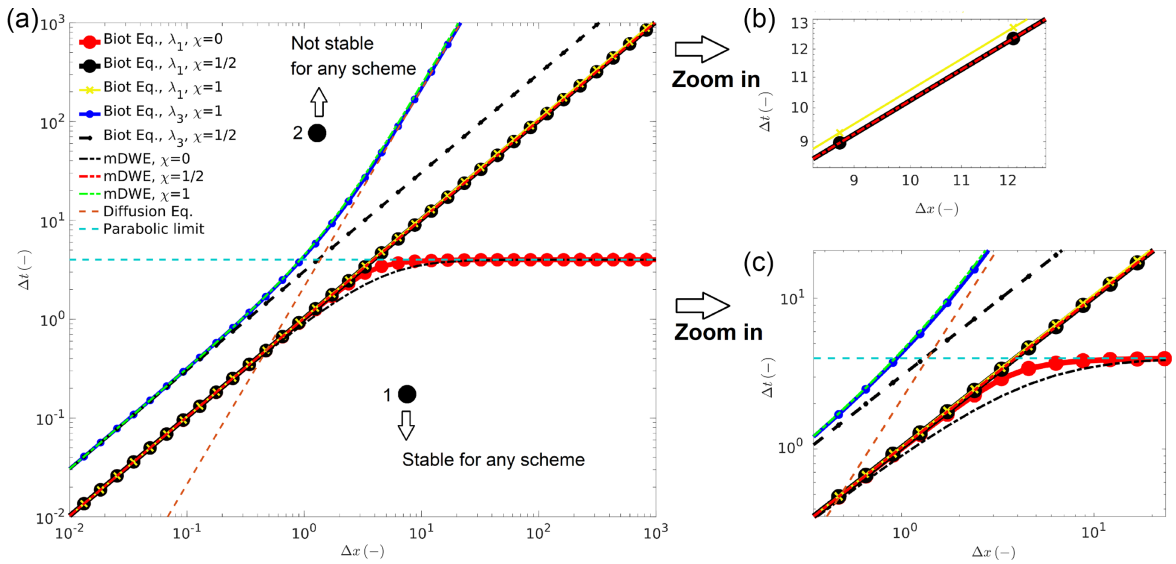

Figure 9. The restrictions on Δt arising from the roots $\gamma_{\overline{1..4}}$ as a function of Δx for Biot's and modified DWE (mDWE) equations. $\lambda_1 = 1$ and $\lambda_3 = 1$ correspond to the positive roots of (57) for positive Δt (a–c). Point 1 is stable for any scheme, point 2 is not stable for any scheme.

The parabolic limit is shown in Fig. 9 (dashed light blue curve).

4.2.2 *Implicit–explicit scheme for Darcy's flux*

We repeat the same procedure for the scheme with $\chi = 1/2$. The roots of the polynomial γ are

$$\gamma_1 = 1/V_1^{HF}, \quad \gamma_3 = 1/V_2^{HF}, \tag{61}$$

where $V_1^{HF} \approx 0.977$, $V_2^{HF} \approx 0.328$. The roots $\gamma_{3,4}$ (61) are less restrictive as the roots $\gamma_{1,2}$. The most restrictive condition for this scheme is represented by γ_1 (61) (Fig. 9, solid black curve)

$$\Delta t \leqslant \Delta x / V_1^{HF}, \tag{62}$$

which is the same as the CFL condition of the wave eq. (10) (taking $V = V_1^{HF}$).

4.2.3 *Implicit scheme for Darcy's flux*

The polynomial γ of the implicit scheme ($\chi = 1$) of Biot's eqs (28)–(29) is

$$\gamma_\xi(z) = 4(105z^4 - 56\Delta x\, z^3 - 68z^2 + 4\Delta x\, z + 4). \tag{63}$$

The root γ_1 varies slightly as a function of Δx. For $\Delta x \ll 1$,

$$\gamma_1 \approx 1/V_1^{HF}, \tag{64}$$

For $\Delta x \gg 1$, the condition is slightly less restrictive. For $\Delta x = 1$,

$$\gamma_1 \approx 1/0.968. \tag{65}$$

The root γ_1 (64) is very close as for the explicit and implicit–explicit schemes for Darcy's flux (see Fig. 9, solid black and solid yellow curves). The roots $\gamma_{\overline{3,4}}$ (64) are calculated numerically by solving (63) and the associated restrictions on Δt are shown in Fig. 9 (solid blue curve). The most restrictive condition for the implicit scheme is represented by the root γ_1 (Fig. 9, solid yellow curve). If $\Delta x \gg 1$, this condition is slightly less restrictive than for the $\chi = 1/2$ scheme, thus the condition (62) is also valid,

$$\Delta t \leqslant \Delta x / V_1^{HF}, \tag{66}$$

which is the same as the CFL condition of the wave eq. (10) (taking $V = V_1^{HF}$). Note, that for large Δx ($\Delta x \gg 1$), the time step can be chosen slightly larger (the difference might be less than 1 per cent) than the time step given by the condition (66) but this is not practical and we do not explore this in more detail.

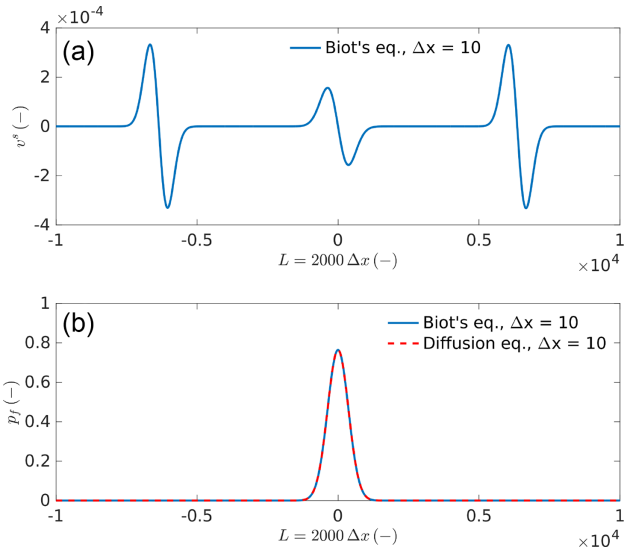

Figure 10. Snapshots of the solid velocity and fluid pressure wavefields of the dimensionless Biot's poroelastic eqs (28)–(29) and for the diffusion equation. Panel (a) shows one propagating wave V_1 and a diffusive mode, which corresponds to V_2. Panel (b) shows the fluid pressure field of Biot's equations (solid blue) and of the diffusion equation (dashed red). The initial condition is given to the fluid pressure p_f of a Gaussian shape. The material parameters are $\zeta_{12} = 1/8$, $\zeta_{22} = 1/4$, $\varrho_{12} = 1/4$, $\varrho_{22} = 1/2$.

Table 3. Summary of CFL conditions for different schemes in Example 2.

Scheme for Darcy's flux	Explicit	Explicit–implicit	Implicit
Scheme for the wave propagation part	Explicit	Explicit	Explicit
CFL condition	Closed-form expression can be always Calculated from the roots of (57). Limits: $\Delta t \leqslant \frac{\Delta x}{V_1^{HF}}$ for $\Delta x \ll 1$ $\Delta t \leqslant \frac{2}{\varrho_{22}}$ for $\Delta x \gg 1$	Exact condition: $\Delta t \leqslant \frac{\Delta x}{V_1^{HF}}$	Very good approximation: $\Delta t \leqslant \frac{\Delta x}{V_1^{HF}}$
Analytical expression for the CFL condition	Exact solution via the Maple script or an approximation by (54)	yes	Exact solution via the Maple script. Almost equivalent to (66)

4.2.4 The modified CFL condition for the DWE

We use the same CFL stability condition (54) of DWE as we used in Example 1 for the explicit scheme ($\chi = 0$). The restriction on Δt from this condition is shown in Fig. 9 (dotted black curve), which coincides with the exact CFL condition for Biot's equations (arriving from (58)) in the high and low frequency limits and slightly diverges in the intermediate regime $\Delta x \in [1, 10]$. Since it diverges to the smaller Δt, the condition of DWE always corresponds to the stable solution of Biot's eqs (28)-(29).

The CFL conditions arising from (A11) considering the implicit–explicit ($\chi = 1/2$) and implicit ($\chi = 1$) schemes are shown in Fig. 9 (dotted red and dotted green curves, respectively). The DWE CFL condition for the implicit–explicit scheme (54) is equivalent to the exact CFL conditions of Biot's equations for scheme with $\chi = 1/2$. The DWE CFL (A11) condition for the implicit scheme (with modifications similar to (54)) is very close to the exact one of Biot's equations with $\chi = 1$ arriving from the root γ_3. This condition is always less restrictive than the CFL condition of the wave eq. (10) (using $V = V_1^{HF}$); thus, does not take effect in Biot's equations if the scheme for the hyperbolic part of Biot's equations is explicit.

The CFL condition of the diffusion eq. (12) is shown in Fig. 9 (dashed brown curve), where the diffusivity D is calculated according to (55). The CFL condition of the diffusion eq. (12) is equivalent to the limit $\Delta x \gg 1$ of the CFL of Biot's equations with $\chi = 1$ arriving from the root γ_3. Furthermore, the fluid pressure field predicted by the diffusion equation is equivalent to the fluid pressure filed of Biot's equations (Fig. 10). The summary of CFL conditions for different schemes for Biot's equations of Example 2 is shown in Table 3.

4.2.5 Back propagation of Biot's equations

The derived CFL conditions for the three schemes of Biot's equations exhibit mirror symmetry along $\Delta t = 0$, similarly to the DWE (Fig. 5). The back propagation of Biot's equations fully depends on the behaviour of the wave of the second kind. If V_2 is a propagating wave, the back propagation is possible. If V_2 is a diffusion process, the back propagation results in growing amplitudes of V_2 at each time step, thus, the

back propagating solution will never converge to the initial state. Similarly to the DWE, the back propagation of Biot's equations is always stable and the physical correctness of the back propagation wavefields purely depends on V_2.

5 DISCRETE SCHEMES OF DIMENSIONAL BIOT'S POROELASTIC EQUATIONS

The first order velocity–stress system of dimensional Biot's equations (Biot 1962) is given in Appendix B (B1–B3). The performed stability analysis for the dimensionless Biot's equations can be applied to the dimensional equations as well. For that, we introduce a set of dimensional material parameters $\hat{\zeta}$ and $\hat{\varrho}$:

$$\hat{\zeta}_{ij} = \begin{pmatrix} K_u + 4/3G & \alpha M \\ \alpha M & M \end{pmatrix}, \quad \hat{\varrho}_{ij} = \frac{1}{\Theta} \begin{pmatrix} \rho_a & \rho_f \\ \rho_f & \rho_t \end{pmatrix}. \tag{67}$$

We also need the determinants of those matrices

$$\det(\hat{\zeta}_{ij}) = \hat{\zeta}_{11}\hat{\zeta}_{22} - \hat{\zeta}_{12}^2, \quad \det(\hat{\varrho}_{ij}) = \hat{\varrho}_{11}\hat{\varrho}_{22} - \hat{\varrho}_{12}^2. \tag{68}$$

and the parameter $\hat{A}$,

$$\hat{A} = \hat{\zeta}_{11}\hat{\varrho}_{11} + \hat{\zeta}_{22}\hat{\varrho}_{22} - 2\hat{\zeta}_{12}\hat{\varrho}_{12}. \tag{69}$$

The dimensional velocity $\hat{V}_1^{HF}$ can be calculated as

$$\hat{V}_1^{HF} = \left(\frac{\hat{A} - \sqrt{\hat{A}^2 - 4\det(\hat{\zeta} ij)\det(\hat{\varrho}_{ij})}}{2\det(\hat{\zeta}_{ij})\det(\hat{\varrho}_{ij})} \right)^{-1/2}. \tag{70}$$

In the previous section, we studied the three schemes, namely, explicit ($\chi = 0$), implicit–explicit ($\chi = 1/2$) and implicit ($\chi = 1$) schemes for Darcy's flux. The explicit scheme is not useful since it dramatically reduces the stable time step in the diffusive regime of the *P*-slow wave. The accuracy determines the choice between the implicit–explicit or implicit schemes for Darcy's flux of Biot's equations. The implicit–explicit scheme is second order accurate in space and time. The implicit scheme provides slightly lower accuracy, around 1.8. Therefore, the $\chi = 1/2$ scheme, described in Section 4.2.2, is the most reasonable choice and the CFL condition for the dimensional case is determined as

$$\Delta t \leqslant \frac{\Delta x}{\hat{V}_1^{HF}}, \tag{71}$$

where $\hat{V}_1^{HF}$ is given by (70). The extension to two-, three- and *n*-dimensions is straightforward

$$\Delta t \leqslant \frac{1}{\hat{V}_1^{HF}\sqrt{\sum_{i=1}^{n} \frac{1}{\Delta x_i^2}}}. \tag{72}$$

If $\Delta x_i = \Delta x$, then

$$\Delta t \leqslant \frac{\Delta x}{\sqrt{n}\,\hat{V}_1^{HF}}, \tag{73}$$

The conditions (71), (72), (73) can be generalized to a fourth-order accurate in space, second-order accurate in time discrete numerical scheme using the coefficients of the fourth-order approximation to the spatial derivatives (Levander 1988; Masson *et al.* 2006).

There is also a criterion on the input material parameters. The stability analysis suggests that the matrices of material parameters $\hat{\zeta}$ and $\hat{\varrho}$ (expression 67) must be positive definite. It is notable that the condition on the matrix $\hat{\zeta}$ (eq. 67) is less restrictive than the condition from the general principles of thermodynamic on the matrix in (B1) (they are equivalent if the shear modulus is zero), thus, the most restrictive condition must be used. The positive definiteness of $\hat{\varrho}$ suggests that all eigenvalues are positive.

Our stability analysis has been performed for homogeneous materials but the results can be applied also for heterogeneous and anisotropic materials. If strong heterogenities and anisotropies are present, the smallest time step should be used for numerical simulations. The smallest time step can be determined by calculating the time step for the most restrictive parameters presented in the model.

In some extreme scenarios, for example, if poroelastic media degenerates into acoustic media at some spatial location and the rest of the model domain is poroelastic, the smallest time step might be reduced by some factor otherwise numerical instabilities might appear. In this extreme case, numerical experiments are needed. Also, if poroelastic media degenerates into acoustic media the matrix $\hat{\zeta}$ (expression 67) becomes singular (all components are the same) while the matrix $\hat{\varrho}$ must be positive definite. In this case, poroelastic equations exactly reproduce acoustic wave propagation in a fluid.

Table 4. Material parameters of a sandstone.

Symbol	Value	Unit
K_g	40	(GPa)
ρ_s	2500	(kg m^{-3})
K_d	20	(GPa)
G	12	(GPa)
ϕ	0.2	(–)
κ	600×10^{-13}	(m^2)
T	2	(–)
K_f	2.5	(GPa)
ρ_f	1000	(kg m^{-3})
η	10^{-3}	(kg (m·s)$^{-1}$)
ω_c	2×10^4	(Hz)
Δt_{st}^{1D}	$4.7045949598862 \times 10^{-6}$	(s)
Δt_{st}^{3D}	$1.0266267865612 \times 10^{-6}$	(s)

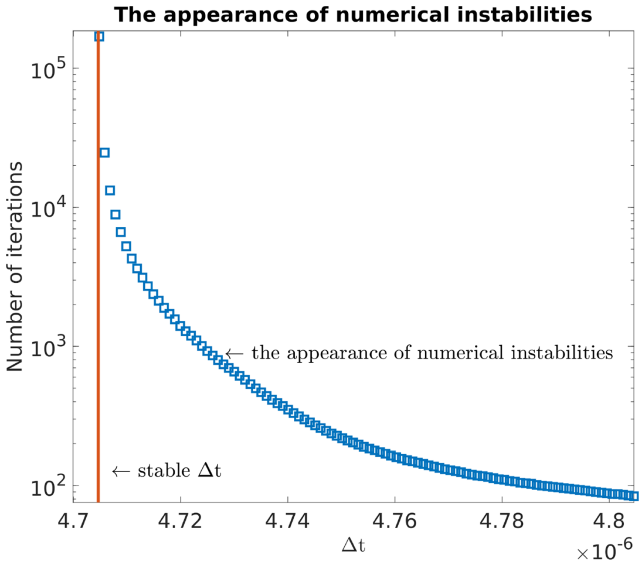

Figure 11. Number of iterations before the numerical instabilities appeared in the 1-D numerical solution of Biot's equations. Each blue square corresponds to the numerical simulation. The material and numerical parameters are given in Table 4.

5.1 Numerical examples

Let us test the derived above CFL conditions. We performed several 1-D, 2-D and 3-D numerical simulations with different time steps. The source is the Ricker wavelet

$$F_R(t_m) = A_0(1 - 2\,(\pi(t_m - t_{m0})\Delta t_{st}\, f_c)^2\; e^{-(\pi(t_m - t_{m0})\Delta t_{st}\, f_c)^2}, \tag{74}$$

where $A_0 = 1/\Delta t_{st}$ is the amplitude of the wavelet, Δt_{st} is the stable time step, $f_c = \omega_s/(2\pi)$ is the frequency of the source wavelet (ω_s is the angular frequency), t_m is the iteration number, t_{m0} is the wavelet delay (in iterations).

5.1.1 1-D numerical experiment

First, we test the 1D CFL condition (71). We use a 1-D domain of 10 m with $\Delta x^{1D} = 0.02$ m resulting in 500 grid cells. We apply the source (74) to the total stress $\bar{\sigma}$. The central frequency of the source wavelet is $f_c = 1 \times 10^4/\pi$ Hz and the wavelet delay is $t_{m0} = 5 \times 10^{-4}/\Delta t_{st}^{1D}$. We perform a set of numerical simulations with different Δt using the parameters given in Table 4. For Δt derived by (71), the scheme is always stable (Fig. 11, brown line). We increase the stable Δt by a small factor $l \cdot 2 \times 10^{-10}$s, where $l \in [1, 500]$ m. The resulting set of different time steps Δt corresponds to the x-axis in Fig. 11. A small increase of the stable Δt by 2×10^{-10}s causes numerical instabilities of the numerical solution after 168 603 time steps. A larger increase of the stable Δt causes numerical instabilities at significantly smaller time steps (blue squares in Fig. 11).

In 2-D or 3-D numerical simulations of Biot's equations, the CFL condition is different from that one of the 1-D case. If the source (or the initial condition) is in the form of a plane wave and is aligned with the grid cells, then the 1-D CFL condition is also valid in 2-D and 3-D. This is due to the fact that the plane wave is a multidimensional source and 1-D, 2-D and 3-D simulations are similar. But once the wave

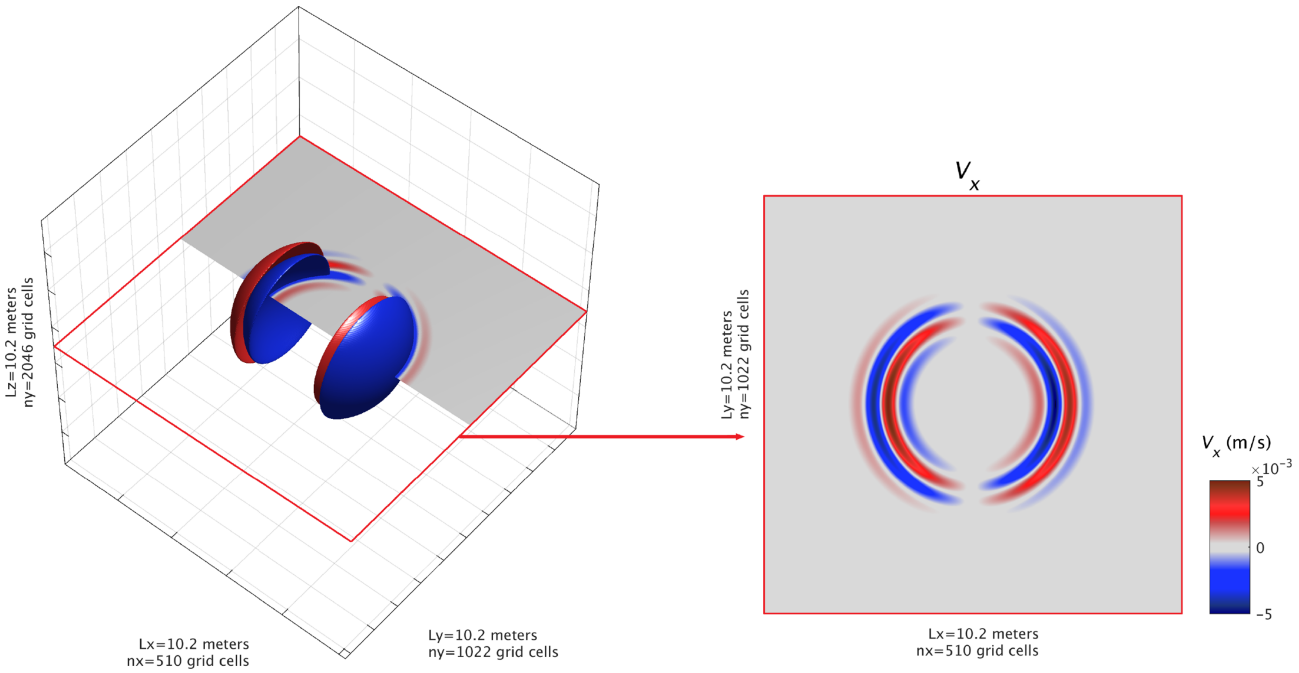

Figure 12. The the solid velocity wave field V_x after 850 time steps. The material and numerical parameters are given in Table 4.

propagation direction becomes different (for example, due to a reflection), the 1-D CFL condition is not longer valid in 2-D and 3-D and the CFL condition (72) should be used.

5.1.2 3-D numerical experiment

We simulate a wave propagating in 3-D for the isotropic poro-elastic material whose properties are given in Table 4. We use the CFL condition (72). A 3-D square domain of 10.2 m × 10.2 m × 10.2 m is used. We set $\Delta x = 0.02$ m, $\Delta y = 0.01$ m and $\Delta z = 0.005$ m. The numerical model consists of 510 × 1022 × 2046 grid cells in x-, y- and z-directions, respectively. The total number of grid cells is $\approx 1 \times 10^9$. The simulations were performed on 8 Tesla V100 32 GB Nvlink GPUs using the message passing interface (MPI) standard, the running time was approximately 55-60 seconds for all simulations. We set a different number of grid cells in different directions for a more precise testing of the CFL condition (72) in 3-D. The central frequency of the source wavelet is $f_c = 4 \times 10^3$ Hz and the wavelet delay is $t_{m0} = 3.3(3) \times 10^4$. The stable Δt is shown in Table 4 as Δt_{st}^{3D}. We multiplied Δt_{st}^{3D} by 0.99 and performed 850 time steps. The the solid velocity wave field V_x is shown in Fig. 12, which obeys a perfect spherical behaviour as expected. In another simulation, we multiplied Δt_{st}^{3D} by 1.01 and the simulation became unstable before 850 time steps.

6 SUMMARY

We performed the von Neumann stability analysis of the elastodynamic Biot's eqs (28)–(29). The characteristic times of the wave propagation (hyperbolic) and diffusion (parabolic) processes are different, thus, the system of equations exhibits a 'stiff' behaviour. The 'stiffness' affects the CFL condition, which is derived for a discrete system of equations. In order to avoid very small time steps, different strategies are needed to discretize the hyperbolic and parabolic operators. We use the discrete scheme (37)–(38), which is explicit for the wave propagation part and varies for the diffusion process described by Darcy's flux. Darcy's flux is discretized using explicit, implicit–explicit and implicit schemes.

We provided the exact CFL conditions of Biot's equations, which are obtained by solving a polynomial of degree four. This polynomial exists for any set of input material and numerical parameters and can be derived analytically using the Maple script provided as supplementary material. Since, the scheme for the wave operator is explicit, the absolute values of the first two roots are determined by the fastest propagating wave. Thus, the CFL condition of Biot's equations is at least that one of the wave eq. (10). The other two roots correspond to the wave of the second kind, which may behave as a propagating wave or as a diffusion process. The CFL condition arriving from the first two roots can be significantly affected by the CFL condition arriving from the third and fourth roots, depending of the scheme for Darcy's flux.

If the scheme for Darcy's flux is explicit, the CFL condition is highly affected. The time step might be very small in the diffusion regime of the slow P wave V_2 and converges to the spectral radius of the parabolic operator (60). But the time step is not affected in the wave propagation regime of the slow P wave V_2 (Fig. 9, solid red curve).

If the scheme for Darcy's flux is implicit–explicit (or implicit), the CFL condition is not affected by the parabolic operator. In this case, the CFL condition of the wave eq. (71) is valid (Fig. 9, solid black curve). Note, that the CFL condition does not depend on viscosity and

permeability of the medium. It is important to note that the fast wave velocity V_1 of Biot's eqs (28)–(29) is different in wave propagation and diffusion regimes of the slow wave V_2. The wave velocity in the CFL condition (10) must be chosen to that one of the high frequency limit V_1^{HF} (31) despite of the propagation or diffusive regime for V_2 for a given simulation. For example, if one solves numerically Biot's equations in the diffusive regime for V_2 (usually corresponds to low frequencies) and uses the CFL condition (10) with the current fastest velocity (36), the solution will be unstable. Thus, the CFL condition (71) with the velocity V_1^{HF} (70) always applies.

7 DISCUSSION

In geophysics, explicit schemes for the wave simulations are very popular but also implicit schemes exist. If an implicit scheme for the wave operator of Biot's equations is used, the restriction on the time step arriving from the wave equations vanishes. In this case, the time step will be determined by the scheme for Darcy's flux. If the scheme for Darcy's flux is also implicit, the scheme will be unconditionally stable and the time step will be determined by the accuracy and computational efficiency. If the scheme for the diffusion part is explicit, the time step will converge to the spectral radius of the parabolic operator (60) in the diffusive regime of the slow *P* wave V_2.

Another common approach to overcome the stiffness of PDEs is based on the operator splitting approach. The idea is that the system of PDEs is separated into the two parts. The first system contains only hyperbolic operators ('non stiff') and is solved using an explicit time integration. The second system contains parabolic operators ('stiff') and is solved independently from the first system at each time step. Operator splitting can be a first order Godunov-type, a second order, for example Strang splitting (Strang 1968), or even higher order approaches exist. In the context of Biot's equations, some authors solve the stiff part analytically (Carcione & Quiroga-Goode 1995; Chiavassa *et al.* 2010; Chiavassa & Lombard 2011). A detailed investigation of the operator splitting approach can be find in (Marchuk 1975; LeVeque *et al.* 2002). In order to converge to the original solution, the usual requirement to the operator splitting approach is that the solution of the system of PDEs is smooth (additionally, other requirements may be needed), which might not be always fulfilled in heterogeneous media. A proper usage of the operator splitting for a system of PDEs should be carefully investigated.

7.1 Comparison with previous works

Masson *et al.* (2006) studied the stability conditions of a *o*(4, 2) (4th order in space and 2nd order in time) numerical scheme for Biot's equations and used the implicit–explicit time integration for Darcy's flux. They derived the 'analytical criterion', which coincides with our result (71) for the implicit–explicit scheme ($\chi = 1/2$). On the other hand, as an approximation (Masson *et al.* 2006) pointed out that the the classic Courant condition $\Delta t \leqslant 1/\hat{V}_1^{LF}$, where $\hat{V}_1^{LF}$ is the undrained fast velocity (36), can be used. Note, that the velocity $\hat{V}_1^{HF}$ is usually 10–20 per cent higher than the $\hat{V}_1^{LF}$ velocity, thus instead, the CFL condition (71) should be used. In addition, Masson *et al.* (2006) obtained the condition for material parameters (densities)

$$(1+\Phi)\frac{T}{\phi} < \frac{\rho_f}{\rho}, \tag{75}$$

where Φ is a positive real dimensionless parameter related to the pore space structure (see Masson *et al.* 2006). In the present notation, the condition (75) can be rewritten as

$$\rho_a \rho - \rho_f^2 > 0. \tag{76}$$

The condition (76) was also suggested by Carcione & Quiroga-Goode (1995) and Wenzlau & Müller (2009). The condition (76) states that the determinant of the matrix $\hat{\varrho}$ (eq. 67) is positive, which is equivalent to the statement that the matrix $\hat{\varrho}^{-1}$ is positive definite (assuming that the diagonal elements are positive).

The derived limits (59 and 60) of the CFL condition of the explicit scheme ($\chi = 0$) of Biot's equations are the same as reported by Chiavassa *et al.* (2010), Chiavassa & Lombard (2011) and Blanc *et al.* (2013) for a slightly different explicit scheme of Biot's equations.

We have not discovered inconsistencies in the von Neumann stability analysis reported by O'Brien (2010). Our analytical derivations using Maple as well as numerical tests show that once the matrices of material parameters are positive definite and the CFL condition on the time step (71) (in 1-D) is fulfilled—the $\chi = 1/2$ discrete scheme for the dynamic Biot's equations is stable over a wide range of material and numerical parameters.

8 CONCLUSIONS

We performed the von Neumann stability analyses of discrete schemes for the elastodynamic Biot's equations. The characteristic times of hyperbolic and parabolic processes are different thus the system of equations exhibits a 'stiff' behaviour. Such 'stiffness' affects the stable time step. We use the explicit scheme for the wave propagation and apply different schemes for Darcy's flux. If the scheme for Darcy's flux is explicit, the stable time step becomes very small in the diffusion regime of the slow *P* wave. If the scheme for Darcy's flux is implicit–explicit or implicit, the stable time step is not affected. In this case, the CFL condition of the discrete Biot's equations coincides with the CFL condition of the wave equation taking the highest fast *P*-wave velocity in the high frequency regime. All the analytical expressions derived for the discrete schemes were verified numerically in one-, two- and three-dimensions.

ACKNOWLEDGEMENTS

Yury Alkhimenkov gratefully acknowledges support from the Swiss National Science Foundation, project number 172691. Yury Alkhimenkov, Lyudmila Khakimova and Yury Y. Podladchikov gratefully acknowledge support from the Ministry of Science and Higher Education of the Russian Federation (project No. 075-15-2019-1890). Yury Alkhimenkov thanks Beatriz Quintal for many suggestions and comments which helped us to improve the quality of the manuscript. Yury Alkhimenkov thanks Ludovic Räss for fruitful discussions regarding the multi-GPU implementation of Biot's equations. The authors thank Philippe Logean for technical support and the Swiss Geocomputing Centre for providing computational resources. We thank Igor Morozov and an anonymous reviewer for many valuable suggestions and recommendations. No data were used in producing this manuscript. For the reproducibility of the presented results, we provide both the Matlab and symbolic Maple routines. These routines are available for download from Bitbucket at https://bitbucket.org/yalkhimenkov/biotcfl/ (last access: 4 December 2020). The routines archive (v1.0) is available from a permanent DOI repository (Zenodo) at http://doi.org/10.5281/zenodo.4304965 (last access: 4 December 2020).

REFERENCES

Alkhimenkov, Y., Khakimova, L. & Podladchikov, Y.Y., 2020. BiotCFL (Version v1.0). Zenodo. http://doi.org/10.5281/zenodo.4304965.

Bause, M., Both, J.W. & Radu, F.A., 2019. Iterative coupling for fully dynamic poroelasticity, preprint (arXiv:1912.05174).

Bause, M., Köcher, U., Radu, F. & Schieweck, F., 2020. Post-processed Galerkin approximation of improved order for wave equations, *Math. Comput.,* **89**(322), 595–627.

Biot, M., 1956. Theory of propagation of elastic waves in a fluid-saturated porous solid. I. Low-frequency range, *J. acoust. Soc. Am.,* **28**(2), 168–178.

Biot, M.A., 1941. General theory of three-dimensional consolidation, *J. Appl. Phys.,* **12**(2), 155–164.

Biot, M.A., 1956. Theory of propagation of elastic waves in a fluid-saturated porous solid. II. Higher frequency range, *J. acoust. Soc. Am.,* **28**(2), 179–191.

Biot, M.A., 1962. Mechanics of deformation and acoustic propagation in porous media, *J. Appl. Phys.,* **33**(4), 1482–1498.

Biot, M.A., 1965. *Mechanics of Incremental Deformations,* John Wiley & Sons.

Biot, M.A. & Willis, D., 1957. The elastic coeff cients of the theory of consolidation, *J. Appl. Mech.,* **15,** 594–601.

Blanc, E., Chiavassa, G. & Lombard, B., 2013. A time-domain numerical modeling of two-dimensional wave propagation in porous media with frequency-dependent dynamic permeability, *J. acoust. Soc. Am.,* **134**(6), 4610–4623.

Boscarino, S. & Russo, G., 2013. Flux-explicit imex Runge–Kutta schemes for hyperbolic to parabolic relaxation problems, *SIAM J. Numer. Anal.,* **51**(1), 163–190.

Carcione, J.M. & Quiroga-Goode, G., 1995. Some aspects of the physics and numerical modeling of Biot compressional waves, *J. Comput. Acoust.,* **3**(04), 261–280.

Chiavassa, G. & Lombard, B., 2011. Time domain numerical modeling of wave propagation in 2D heterogeneous porous media, *J. Comput. Phys.,* **230**(13), 5288–5309.

Chiavassa, G., Lombard, B. & Piraux, J., 2010. Numerical modeling of 1D transient poroelastic waves in the low-frequency range, *J. Comput. Appl. Math.,* **234**(6), 1757–1765.

Dai, N., Vafidis, A. & Kanasewich, E., 1995. Wave propagation in heterogeneous, porous media: a velocity-stress, finite-difference method, *Geophysics,* **60**(2), 327–340.

de la Puente, J., Dumbser, M., Käser, M. & Igel, H., 2008. Discontinuous Galerkin methods for wave propagation in poroelastic media, *Geophysics,* **73**(5), T77–T97.

Ding, H.-f., Zhang, Y.-x., Cao, J.-x. & Tian, J.-h., 2012. A class of difference scheme for solving telegraph equation by new non-polynomial spline methods, *Appl. Math. Comput.,* **218**(9), 4671–4683.

Dormy, E. & Tarantola, A., 1995. Numerical simulation of elastic wave propagation using a finite volume method, *J. geophys. Res.,* **100**(B2), 2123–2133.

Ernesti, J. & Wieners, C., 2019. A space-time discontinuous Petrov–Galerkin method for acoustic waves, in *Space-Time Methods*, pp. 89–116, eds Ulrich Langer and Olaf, De Gruyter, doi:0.1515/9783110548488-003.

Frenkel, J., 1944. On the theory of seismic and seismoelectric phenomena in a moist soil, *J. Phys.,* **III**(4), 230–241.

Gregor, D., Moczo, P., Kristek, J., Mesgouez, A., Lefeuve-Mesgouez, G. & Kristekova, M., 2021. Subcell-resolution finite-difference modelling of seismic waves in Biot and JKD poroelastic media *Geophys. J. Int.,* **224**(2), 760–794.

Hetnarski, R.B. & Ignaczak, J., 1999. Generalized thermoelasticity, *J. Therm. Stress.,* **22**(4–5), 451–476.

Hirsch, C., 1988. *Numerical Computation of Internal and External Flows, Vol. 1: Fundamentals of Numerical Discretization,* John Wiley and Sons.

Jin, S. & Levermore, C.D., 1996. Numerical schemes for hyperbolic conservation laws with stiff relaxation terms, *J. Comput. Phys.,* **126**(2), 449–467.

Jordan, P. & Puri, A., 1999. Digital signal propagation in dispersive media, *J. appl. Phys.,* **85**(3), 1273–1282.

Kolesov, A.E., Vabishchevich, P.N. & Vasilyeva, M.V., 2014. Splitting schemes for poroelasticity and thermoelasticity problems, *Comput. Math. Appl.,* **67**(12), 2185–2198.

Köcher, U. & Bause, M., 2014. Variational space–time methods for the wave equation, *J. Scient. Comput.,* **61**(2), 424–453.

Lemoine, G.I., 2016. Three-dimensional mapped-grid finite volume modeling of poroelastic-fluid wave propagation, *SIAM J. Scient. Comput.,* **38**(5), B808–B836.

Lemoine, G.I., Ou, M.Y. & LeVeque, R.J., 2013. High-resolution finite volume modeling of wave propagation in orthotropic poroelastic media, *SIAM J. Scient. Comput.,* **35**(1), B176–B206.

Levander, A.R., 1988. Fourth-order finite-difference P-SV seismograms, *Geophysics,* **53**(11), 1425–1436.

LeVeque, R.J. *et al.*, 2002. *Finite Volume Methods for Hyperbolic Problems,* Vol. **31,** Cambridge Univ. Press.

Macías-Díaz, J. & Puri, A., 2010. A boundedness-preserving finite-difference scheme for a damped nonlinear wave equation, *Appl. Numer. Math.,* **60**(9), 934–948.

Marchuk, G.I., 1975, *Methods of Numerical Mathematics,* Springer-Verlag New York.

Masson, Y.J., Pride, S. & Nihei, K., 2006. Finite difference modeling of Biot's poroelastic equations at seismic frequencies, *J. geophys. Res.,* **111**(B10), doi:10.1029/2006JB004366.

Mickens, R.E. & Jordan, P., 2004. A positivity-preserving nonstandard finite difference scheme for the damped wave equation, *Numer. Methods Partial Different. Eq.,* **20**(5), 639–649.

Moczo, P., Gregor, D., Kristek, J., & de la Puente, J., 2019. A discrete representation of material heterogeneity for the finite-difference modelling of seismic wave propagation in a poroelastic medium, *Geophysical Journal International,* **216**(2), 1072–1099.

Mohanty, R., 2004. An unconditionally stable difference scheme for the one-space-dimensional linear hyperbolic equation, *Appl. Math. Lett.,* **17**(1), 101–105.

Morency, C. & Tromp, J., 2008. Spectral-element simulations of wave propagation in porous media, *Geophys. J. Int.,* **175**(1), 301–345.

Najafi, H.S. & Izadi, F., 2014. Comparison of two finite-difference methods for solving the damped wave equation, *Int. J. Math. Eng. Sci.,* **3,** 35–49.

O'Brien, G.S., 2010. 3d rotated and standard staggered finite-difference solutions to Biots poroelastic wave equations: stability condition and dispersion analysis, *Geophysics,* **75**(4), T111–T119.

Pareschi, L. & Russo, G., 2005. Implicit–explicit Runge–Kutta schemes and applications to hyperbolic systems with relaxation, *J. Scient. Comp.,* **25**(1), 129–155.

Pascal, H., 1986. Pressure wave propagation in a fluid flowing through a porous medium and problems related to interpretation of Stoneley's wave attenuation in acoustical well logging, *Int. J. Eng. Sci.,* **24**(9), 1553–1570.

Schieweck, F., 2010. A-stable discontinuous Galerkin–Petrov time discretization of higher order, *J. Numer. Math.,* **18**(1), 25–57.

Shukla, K., Chan, J., Maarten, V. & Jaiswal, P., 2020. A weight-adjusted discontinuous Galerkin method for the poroelastic wave equation: penalty fluxes and micro-heterogeneities, *J. Comput. Phys.,* **403,** 109061.

Strang, G., 1968. On the construction and comparison of difference schemes, *SIAM J. Numer. Anal.,* **5**(3), 506–517.

Virieux, J., 1986. P-SV wave propagation in heterogeneous media: velocity-stress finite-difference method, *Geophysics,* **51**(4), 889–901.

Virieux, J. & Madariaga, R., 1982. Dynamic faulting studied by a finite difference method, *Bull. seism. Soc. Am.,* **72**(2), 345–369.

Ward, N.D., Lähivaara, T. & Eveson, S., 2017. A discontinuous Galerkin method for poroelastic wave propagation: the two-dimensional case, *J. Comput. Phys.,* **350,** 690–727.

Wenzlau, F. & Müller, T.M., 2009. Finite-difference modeling of wave propagation and diffusion in poroelastic media, *Geophysics,* **74**(4), T55–T66.

Zeng, Y., He, J. & Liu, Q., 2001. The application of the perfectly matched layer in numerical modeling of wave propagation in poroelastic media, *Geophysics,* **66**(4), 1258–1266.

Zhan, Q., Zhuang, M., Fang, Y., Hu, Y., Mao, Y., Huang, W.-F., Zhang, R., Wang, D. & Liu, Q.H., 2019. Full-anisotropic poroelastic wave modeling: a discontinuous Galerkin algorithm with a generalized wave impedance, *Comp. Methods Appl. Mech. Eng.,* **346,** 288–311.

Zhu, X. & McMechan, G., 1991. Numerical simulation of seismic responses of poroelastic reservoirs using Biot theory, *Geophysics,* **56**(3), 328–339.

Özdenvar, T. & McMechan, G.A., 1997. Algorithms for staggered-grid computations for poroelastic, elastic, acoustic, and scalar wave equations, *Geophys. Prospect.,* **45**(3), 403–420.

Yarushina, V.M. & Podladchikov, Y.Y., 2015. (De)compaction of porous viscoelastoplastic media: Model formulation, *J. Geophys. Res. Solid Earth,* **120,** 4146–4170.

APPENDIX A: THE DIMENSIONAL DAMPED LINEAR WAVE EQUATION

A.1 Explicit scheme for Darcy's flux

The von Neumann stability analysis for the discrete system (9) suggests that

$$\Delta t \leqslant \Delta x \frac{-\Delta x\,\rho + \sqrt{(\Delta x\,\rho)^2 + 16K\rho\,\tau^2}}{4K\tau}, \tag{A1}$$

which is the exact CFL condition of the discrete scheme (9). Let us analyse the result (A1).

A.2 Wave propagation regime of the explicit scheme

Lets us write a series expansion of the R.H.S. of (A1) assuming $\Delta x \to +0$ (equivalent to assuming $\tau \to +\infty$),

$$\Delta x \frac{-\Delta x\,\rho + \sqrt{(\Delta x\,\rho)^2 + 16K\rho\,\tau^2}}{4K\tau} = \frac{\sqrt{\rho}}{\sqrt{K}}\Delta x - \frac{1}{4}\frac{\rho}{K\tau}(\Delta x)^2 + \frac{1}{32}\frac{\sqrt{K\rho}\,\rho}{K^2\tau^2}(\Delta x)^3 + O((\Delta x)^5). \tag{A2}$$

It can be seen form (A2) that the limit of the R.H.S. of (A1) as $\tau \to +\infty$ is

$$\lim_{\tau\to+\infty} \Delta x \frac{-\Delta x\,\rho + \sqrt{(\Delta x\,\rho)^2 + 16K\rho\,\tau^2}}{4K\tau} = \Delta x \frac{\sqrt{\rho}}{\sqrt{K}} \equiv \frac{\Delta x}{V}, \tag{A3}$$

where $V = \sqrt{K/\rho}$. This CFL condition corresponds to the hyperbolic limit and is valid when $\tau \gg 1$. One can also take into account one more term in the series expansion (A2) and the inequality (A1) becomes

$$\Delta t \leqslant \frac{\Delta x}{V} - \frac{1}{4}\frac{1}{V^2\tau}(\Delta x)^2. \tag{A4}$$

A.3 Diffusive regime of the explicit scheme

Now we consider an opposite scenario. We write a series expansion of the R.H.S of (A1) assuming $\Delta x \to +\infty$ (equivalent to assuming $\tau \to +0$),

$$\Delta x \frac{-\Delta x\,\rho + \sqrt{(\Delta x\,\rho)^2 + 16K\rho\,\tau^2}}{4K\tau} = 2\tau - \frac{8K}{\rho\,(\Delta x)^2}\tau^3 + O(\frac{1}{(\Delta x)^4}). \tag{A5}$$

It is interesting that the first term in the R.H.S of (A5) does not depend on Δx. Thus, when $\tau \to +0$, the stability conditions reads

$$\Delta t \leqslant 2\tau, \tag{A6}$$

which corresponds to the parabolic limit and is valid when $\tau \ll 1$. One can also take into account one more term in the series expansion (A5) and the inequality (A6) becomes

$$\Delta t \leqslant 2\tau - \frac{8K}{\rho\,(\Delta x)^2}\tau^3. \tag{A7}$$

Table A1. List of principal notation.

Symbol	Meaning	Unit
σ^s, σ^f	solid and fluid stresses	(Pa)
τ^s, τ^f	solid and fluid stress deviators	(Pa)
$\bar{p}$, p_f	total and fluid pressures	(Pa)
v^s, v^f	solid and fluid velocities	(m s^{-1})
ρ_s, ρ_f	solid and fluid densities	(kg m^{-3})
K_g, K_f	elastic solid and fluid bulk moduli	(Pa)
G	elastic drained shear moduli	(Pa)
K_d, K_u	elastic drained and undrained bulk moduli	(Pa)
η	fluid shear viscosity	(Pa·s)
κ	permeability	(m^2)
ϕ	porosity	(–)
T	tortuosity	(–)
$\bar{\sigma}$	$=(1-\phi)\sigma^s+\phi\sigma^f$, total stress	(Pa)
$\bar{\tau}$	$=(1-\phi)\bar{\tau}+\phi\tau^f$, total stress deviator	(Pa)
q^D	$=\phi(v^f-v^s)$, Darcy's flux	(m s^{-1})
ρ_t	$=(1-\phi)\rho+\phi\rho$, total density	(kg m^{-3})
α	Biot–Willis coefficient	(–)

A.4 Implicit and implicit–explicit schemes for Darcy's flux

The discrete system of (9) is written as

$$\begin{cases} \dfrac{1}{K}\dfrac{p_i^{l+1/2}-p_i^{l-1/2}}{\Delta t} = -\dfrac{q_{i+1/2}^{l}-q_{i-1/2}^{l}}{\Delta x} \\ \dfrac{q_{i+1/2}^{l+1}-q_{i+1/2}^{l}}{\Delta t} = -\dfrac{1}{\rho}\dfrac{p_{i+1}^{l+1/2}-p_i^{l+1/2}}{\Delta x} - \dfrac{1}{\tau}\left(\chi\, q_{i+1/2}^{l+1}+(1-\chi)\, q_{i+1/2}^{l}\right). \end{cases} \tag{A8}$$

If $\chi = 1/2$, then (A8) corresponds to the implicit–explicit scheme. The von Neumann stability analysis for the discrete system (9) suggests that

$$\Delta t \leqslant \frac{\Delta x}{V}, \tag{A9}$$

where $V=\sqrt{K/\rho}$ is the fast wave velocity.

If $\chi = 1$, then (A8) corresponds to the implicit scheme for Darcy's flux. The von Neumann stability analysis for this scheme suggests that

$$\Delta t \leqslant \Delta x\, \frac{\Delta x\,\rho+\sqrt{(\Delta x\,\rho)^2+16K\rho\,\tau^2}}{4K\tau}, \tag{A10}$$

which is the exact CFL condition of the discrete scheme (A8) with $\chi = 1$.

The general CFL condition of the dimensional linear damped wave eq. (9) can be written as a function of the parameter χ, which defines the ratio of explicit to implicit schemes. For positive Δt, the CFL condition is

$$\Delta t \leqslant \Delta x\, \frac{\dfrac{1}{V}\sqrt{4\left(\chi-\dfrac{1}{2}\right)^2(\Delta x)^2\dfrac{1}{V^2}+16\,\tau^2}+2\left(\chi-\dfrac{1}{2}\right)\dfrac{1}{V^2}\Delta x}{4\tau}, \tag{A11}$$

for negative Δt, the CFL condition is

$$\Delta t \leqslant \Delta x\, \frac{-\dfrac{1}{V}\sqrt{4\left(\chi-\dfrac{1}{2}\right)^2(\Delta x)^2\dfrac{1}{V^2}+16\,\tau^2}+2\left(\chi-\dfrac{1}{2}\right)\dfrac{1}{V^2}\Delta x}{4\tau}. \tag{A12}$$

APPENDIX B: DIMENSIONAL ANALYSIS OF THE ELASTODYNAMIC BIOT'S EQUATIONS

The first order velocity–stress system of Biot's equations can be written as (Biot 1962)

$$\begin{pmatrix} \dfrac{\partial \bar{p}}{\partial t} \\ \dfrac{\partial p_f}{\partial t} \end{pmatrix} = -\begin{pmatrix} K_u & \alpha M \\ \alpha M & M \end{pmatrix}\begin{pmatrix} \nabla_k v_k^s \\ \nabla_k q_k^D \end{pmatrix}, \tag{B1}$$

$$\frac{\partial \bar{\tau}_{ij}}{\partial t} = 2G\left(\frac{1}{2}(\nabla_i v_j^s+\nabla_j v_i^s)-\frac{1}{3}(\nabla_k v_k^s)\delta_{ij}\right) \tag{B2}$$

and

$$\begin{pmatrix} \frac{\partial v_i^s}{\partial t} \\ -\frac{\partial q_i^D}{\partial t} \end{pmatrix} = \frac{1}{\Theta} \begin{pmatrix} \rho_a & \rho_f \\ \rho_f & \rho_t \end{pmatrix} \begin{pmatrix} \nabla_j \left(-\bar{p}\delta_{ij} + \bar{\tau}_{ij}\right) \\ \frac{\eta}{\kappa} q_i^D + \nabla_i p_f \end{pmatrix}, \tag{B3}$$

where $\rho_a = \rho_f T/\phi$ and $\Theta = \rho_t \rho_a - \rho_f^2$. The list of field variables and material parameters is given in Table A1. From the general principles of thermodynamic (e.g.,Yarushina & Podladchikov 2015), the matrices of coefficients in (B1) and (B3) must be positive definite. For an isotropic material saturated with a single fluid, in which the solid frame consists of a single isotropic mineral, the Biot–Willis coefficient is

$$\alpha = 1 - K_d/K_g \tag{B4}$$

where K_u is the undrained bulk modulus

$$K_u = K_d + \alpha^2 M. \tag{B5}$$

M is the fluid storage coefficient

$$M = \left(\phi/K_f + (1-\phi)/K_g - K_d/K_g^2\right)^{-1} \tag{B6}$$

Dimensional analysis is a very powerful method to analyse PDEs and to understand how different physical parameters affect the physical system. For simplicity, a one dimensional example is considered, so the total stress tensor can be written instead of the volumetric and deviatoric stresses. The governing first order velocity–stress system of equations in one space dimension can be written as

$$\begin{pmatrix} \frac{\partial \bar{\sigma}}{\partial t} \\ -\frac{\partial p_f}{\partial t} \end{pmatrix} = \begin{pmatrix} K_u + 4/3G & \alpha M \\ \alpha M & M \end{pmatrix} \begin{pmatrix} \frac{\partial v^s}{\partial x} \\ \frac{\partial q^D}{\partial x} \end{pmatrix}, \tag{B7}$$

$$\begin{pmatrix} \frac{\partial v^s}{\partial t} \\ -\frac{\partial q^D}{\partial t} \end{pmatrix} = \frac{1}{\Theta} \begin{pmatrix} \rho_a & \rho_f \\ \rho_f & \rho_t \end{pmatrix} \begin{pmatrix} \frac{\partial \bar{\sigma}}{\partial x} \\ \frac{\eta}{\kappa} q^D + \frac{\partial p_f}{\partial x} \end{pmatrix}. \tag{B8}$$

Let us define the undrained P-wave modulus as

$$c_{11}^u = (K_u + 4/3G), \tag{B9}$$

which has dimensions of [Pa]. By using the two base quantities — the stiffness c_{11}^u [Pa] and density ρ_a $\left[\mathrm{kg/m^3}\right]$, eqs (B7) and (B8) can be transformed into a dimensionless from. First, the two base quantities c_{11}^u and ρ_a are carried out of parentheses in eqs (B7) and (B8), which can be rewritten as

$$\begin{pmatrix} \frac{\partial \bar{\sigma}}{\partial t} \\ -\frac{\partial p_f}{\partial t} \end{pmatrix} = c_{11}^u \begin{pmatrix} 1 & \alpha M/c_{11}^u \\ \alpha M/c_{11}^u & M/c_{11}^u \end{pmatrix} \begin{pmatrix} \frac{\partial v^s}{\partial x} \\ \frac{\partial q^D}{\partial x} \end{pmatrix}, \tag{B10}$$

$$\begin{pmatrix} \frac{\partial v^s}{\partial t} \\ -\frac{\partial q^D}{\partial t} \end{pmatrix} = \tilde{\rho_a} \begin{pmatrix} 1 & \rho_f/\rho_a \\ \rho_f/\rho_a & \rho_t/\rho_a \end{pmatrix} \begin{pmatrix} \frac{\partial \bar{\sigma}}{\partial x} \\ \frac{\eta}{\kappa} q^D + \frac{\partial p_f}{\partial x} \end{pmatrix}, \tag{B11}$$

where $\tilde{\rho_a} = \rho_a/\Theta$. Then, the following replacements are done

$$\bar{\sigma} \longrightarrow c_{11}^u \tilde{\bar{\sigma}}, \quad p_f \longrightarrow c_{11}^u \tilde{p}_f, \tag{B12}$$

$$v^s \longrightarrow \frac{L_x^*}{\tau^*} \tilde{v}^s, \quad q^D \longrightarrow \frac{L_x^*}{\tau^*} \tilde{q}^D, \tag{B13}$$

$$x \longrightarrow L_x^* \tilde{x}, \quad t \longrightarrow \tau^* \tilde{t}, \tag{B14}$$

where L_x^* [m] is the characteristic length and τ^* [s] is the characteristic time. The resulting system of equations is

$$\begin{pmatrix} \frac{\partial \tilde{\bar{\sigma}}}{\partial \tilde{t}} \\ -\frac{\partial \tilde{p}_f}{\partial \tilde{t}} \end{pmatrix} = \begin{pmatrix} 1 & \tilde{\alpha} \\ \tilde{\alpha} & \tilde{M} \end{pmatrix} \begin{pmatrix} \frac{\partial \tilde{v}^s}{\partial \tilde{x}} \\ \frac{\partial \tilde{q}^D}{\partial \tilde{x}} \end{pmatrix}, \tag{B15}$$

$$(I_1)^2 \begin{pmatrix} \frac{\partial \tilde{v}^s}{\partial \tilde{t}} \\ -\frac{\partial \tilde{q}^D}{\partial \tilde{t}} \end{pmatrix} = \begin{pmatrix} 1 & \tilde{\varrho}_f \\ \tilde{\varrho}_f & \tilde{\varrho}_t \end{pmatrix} \begin{pmatrix} \frac{\partial \tilde{\bar{\sigma}}}{\partial \tilde{x}} \\ I_2 \tilde{q}^D + \frac{\partial \tilde{p}_f}{\partial \tilde{x}} \end{pmatrix}, \tag{B16}$$

where $\tilde{\alpha} = \alpha M/c_{11}^u$, $\tilde{M} = M/c_{11}^u$, $\tilde{\varrho}_f \equiv \rho_f/\rho_a$, $\tilde{\varrho}_t \equiv \rho_t/\rho_a$,

$$I_1 = \sqrt{\frac{1}{\tilde{\rho}_a c_{11}^u}} \frac{L_x^*}{\tau^*}, \tag{B17}$$

and

$$I_2 = \frac{\eta}{\kappa}\frac{1}{c_{11}^u}\frac{(L_x^*)^2}{\tau^*} \tag{B18}$$

The four dimensionless parameters $\tilde{\alpha}$, $\tilde{M}$, $\tilde{\varrho}_f$ and $\tilde{\varrho}_t$ define the coupling between the solid and fluid phases. The two dimensionless parameters I_1, I_2 are the key parameters denoting the ratio between the advection and diffusion time scales. The dimensionless quantities I_1 and I_2 are related to hyperbolic (advection) and parabolic (diffusion) processes, respectively. In order to further reduce the number of parameters, we set $I_1 = 1$. Thus, $L_x^* = \tau^*\sqrt{\tilde{\rho}_a\, c_{11}^u}$ and eq. (B18) becomes

$$I_2 = \frac{\eta}{\kappa}\tilde{\rho}_a\tau^*, \tag{B19}$$

where τ^* is a free parameter. Let us choose τ^* as

$$\tau^* = \left(\frac{\eta}{\kappa}\tilde{\rho}_a\right)^{-1}. \tag{B20}$$

Now, eq. (B19) becomes

$$I_2 \equiv \frac{\eta}{\kappa}\tilde{\rho}_a\tau^* = \frac{\eta}{\kappa}\tilde{\rho}_a\left(\frac{\eta}{\kappa}\tilde{\rho}_a\right)^{-1} \equiv 1 \tag{B21}$$

Therefore, taking into account that $I_1 = 1$ and $I_2 = 1$, the system (B15)–(B16) can be rewritten as

$$\begin{pmatrix} \dfrac{\partial\tilde{\tilde{\sigma}}}{\partial\tilde{t}} \\ -\dfrac{\partial\tilde{p}_f}{\partial\tilde{t}} \end{pmatrix} = \begin{pmatrix} 1 & \tilde{\alpha} \\ \tilde{\alpha} & \tilde{M} \end{pmatrix}\begin{pmatrix} \dfrac{\partial\tilde{v}^s}{\partial\tilde{x}} \\ \dfrac{\partial\tilde{q}^D}{\partial\tilde{x}} \end{pmatrix}, \tag{B22}$$

$$\begin{pmatrix} \dfrac{\partial\tilde{v}^s}{\partial\tilde{t}} \\ -\dfrac{\partial\tilde{q}^D}{\partial\tilde{t}} \end{pmatrix} = \begin{pmatrix} 1 & \tilde{\varrho}_f \\ \tilde{\varrho}_f & \tilde{\varrho}_t \end{pmatrix}\begin{pmatrix} \dfrac{\partial\tilde{\tilde{\sigma}}}{\partial\tilde{x}} \\ \tilde{q}^D + \dfrac{\partial\tilde{p}_f}{\partial\tilde{x}} \end{pmatrix}, \tag{B23}$$

The system of eqs (B22) and (B23) defines the dimensionless elastodynamic Biot's equations for an isotropic medium saturated with a single fluid, where the only for dimensionless parameters are present ($\tilde{\alpha}$, $\tilde{M}$, $\tilde{\varrho}_f$ and $\tilde{\varrho}_t$). Note, that the presented dimensionless analysis is particularly useful for the stability analysis, since we have 1 in the main diagonals of (B22) and (B23). A much better dimensionless analysis can be performed by using the undrained P-wave modulus $c_{11}^d = (K_d + 4/3G)$ and ρ_t as two base quantities.

APPENDIX C: THE AMPLIFICATION MATRICES FOR DIFFERENT SCHEMES FOR EXAMPLE 1

The amplification matrix F for the explicit scheme is

$$F = \begin{bmatrix} -3r^2+1 & 0 & 2\,Ir & Ir \\ 0 & -3r^2+1 & -Ir & 3/2\,Ir^2\Delta x - 2\,Ir \\ 2\,Ir & Ir & 1 & 1/2\,\Delta x\, r \\ -Ir & -2\,Ir & 0 & -dx\,r+1 \end{bmatrix}, \tag{C1}$$

where $r = \Delta t\ \sin(1/2\,\omega)/\Delta x$. We add $\sin(1/2\,\omega)$ in order to avoid cos and sin functions in the resulting solutions. The stability of the explicit scheme is shown in Section 4.1.1.

The amplification matrix F for the implicit–explicit scheme is

$$F = \begin{bmatrix} -3r^2+1 & 0 & 2\,Ir & Ir \\ 3/2\,\frac{dx\,r^3}{\Delta x\,r+2} & -1/2\,\frac{-2\,\Delta x\,r+12r^2-4}{\Delta x\,r+2} & -1/2\,\frac{2\,I\Delta x\,r^2+4\,Ir}{\Delta x\,r+2} & -1/2\,\frac{-2\,I\Delta x\,r^2+8\,Ir}{\Delta x\,r+2} \\ 1/2\,\frac{3\,I\Delta x\,r^2+8\,Ir}{\Delta x\,r+2} & \frac{2\,Ir}{\Delta x\,r+2} & 1/2\,\frac{2\,\Delta x\,r+4}{\Delta x\,r+2} & \frac{\Delta x\,r}{\Delta x\,r+2} \\ \frac{-2\,Ir}{\Delta x\,r+2} & \frac{-4\,Ir}{\Delta x\,r+2} & 0 & -\frac{\Delta x\,r-2}{\Delta x\,r+2} \end{bmatrix}, \tag{C2}$$

where $r = \Delta t\,sin(1/2\,\omega)/\Delta x$. The stability of the implicit–explicit scheme is shown in Section 4.1.2.

The amplification matrix F for the implicit scheme is

$$F = \begin{bmatrix} -3r^2+1 & 0 & 2\,Ir & Ir \\ 3/2\,\frac{\Delta x\,r^3}{\Delta x\,r+1} & -1/2\,\frac{-2\,\Delta x\,r+6r^2-2}{\Delta x\,r+1} & -1/2\,\frac{2\,I\Delta x\,r^2+2\,Ir}{\Delta x\,r+1} & -1/2\,\frac{I\Delta x\,r^2+4\,Ir}{\Delta x\,r+1} \\ 1/2\,\frac{3\,I\Delta x\,r^2+4\,Ir}{\Delta x\,r+1} & \frac{ir}{\Delta x\,r+1} & 1/2\,\frac{2\,\Delta x\,r+2}{\Delta x\,r+1} & 1/2\,\frac{\Delta x\,r}{\Delta x\,r+1} \\ \frac{-Ir}{\Delta x\,r+1} & \frac{-2\,Ir}{\Delta x\,r+1} & 0 & (\Delta x\,r+1)^{-1} \end{bmatrix}, \tag{C3}$$

where $r = \Delta t\,sin(1/2\,\omega)/\Delta x$. The stability of the implicit–explicit scheme is shown in Section 4.1.3.